Characterization of M116.1p, a Murine Cytomegalovirus Protein Required for Efficient Infection of Mononuclear Phagocytes

Ružić, Tina; Juranić Lisnić, Vanda; Mahmutefendić Lučin, Hana; Lenac Roviš, Tihana; Železnjak, Jelena; Cokarić Brdovčak, Maja; Vrbanović, Ana; Oreb, Deni; Kveštak, Daria; Gotovac Jerčić, Kristina; ...

Source / Izvornik: **Journal of Virology, 2022, 96**

Journal article, Published version
Rad u časopisu, Objavljena verzija rada (izdavačev PDF)

https://doi.org/10.1128/JVI.00876-21

Permanent link / Trajna poveznica: https://urn.nsk.hr/urn:nbn:hr:184:065611

AMERICAN SOCIETY FOR MICROBIOLOGY | Journal of Virology®

VIRUS-CELL INTERACTIONS

Characterization of M116.1p, a Murine Cytomegalovirus Protein Required for Efficient Infection of Mononuclear Phagocytes

Tina Ružić,[a] Vanda Juranić Lisnić,[a,b] Hana Mahmutefendić Lučin,[c] Tihana Lenac Roviš,[a] Jelena Železnjak,[a,b] Maja Cokarić Brdovčak,[a,b] Ana Vrbanović,[a,b] Deni Oreb,[a] Daria Kveštak,[a,b] Kristina Gotovac Jerčić,[d,e] Fran Borovečki,[d,e] Pero Lučin,[c] Barbara Adler,[f] Stipan Jonjić,[a,b] Berislav Lisnić[a,b]

[a]Center for Proteomics, Faculty of Medicine, University of Rijeka, Rijeka, Croatia
[b]Department of Histology and Embryology, Faculty of Medicine, University of Rijeka, Rijeka, Croatia
[c]Department of Physiology and Immunology, Faculty of Medicine, University of Rijeka, Rijeka, Croatia
[d]Department of Neurology, University Hospital Center Zagreb, Zagreb, Croatia
[e]Department for Functional Genomics, Center for Translational and Clinical Research, University of Zagreb, School of Medicine and University Hospital Center Zagreb, Zagreb, Croatia
[f]Max von Pettenkofer Institute & Gene Center, Virology, Faculty of Medicine, LMU Munich, Munich, Germany

Tina Ružić and Vanda Juranić Lisnić contributed equally to this article. Author order was determined by the number of experiments in which they were involved.

ABSTRACT Broad tissue tropism of cytomegaloviruses (CMVs) is facilitated by different glycoprotein entry complexes, which are conserved between human CMV (HCMV) and murine CMV (MCMV). Among the wide array of cell types susceptible to the infection, mononuclear phagocytes (MNPs) play a unique role in the pathogenesis of the infection as they contribute both to the virus spread and immune control. CMVs have dedicated numerous genes for the efficient infection and evasion of macrophages and dendritic cells. In this study, we have characterized the properties and function of *M116*, a previously poorly described but highly transcribed MCMV gene region that encodes M116.1p, a novel protein necessary for the efficient infection of MNPs and viral spread *in vivo*. Our study further revealed that M116.1p shares similarities with its positional homologs in HCMV and RCMV, UL116 and R116, respectively, such as late kinetics of expression, N-glycosylation, localization to the virion assembly compartment, and interaction with gH—a member of the CMVs fusion complex. This study, therefore, expands our knowledge about virally encoded glycoproteins that play important roles in viral infectivity and tropism.

IMPORTANCE Human cytomegalovirus (HCMV) is a species-specific herpesvirus that causes severe disease in immunocompromised individuals and immunologically immature neonates. Murine cytomegalovirus (MCMV) is biologically similar to HCMV, and it serves as a widely used model for studying the infection, pathogenesis, and immune responses to HCMV. In our previous work, we have identified the *M116* ORF as one of the most extensively transcribed regions of the MCMV genome without an assigned function. This study shows that the M116 locus codes for a novel protein, M116.1p, which shares similarities with UL116 and R116 in HCMV and RCMV, respectively, and is required for the efficient infection of mononuclear phagocytes and virus spread *in vivo*. Furthermore, this study establishes the α-M116 monoclonal antibody and MCMV mutants lacking M116, generated in this work, as valuable tools for studying the role of macrophages and dendritic cells in limiting CMV infection following different MCMV administration routes.

KEYWORDS cytomegalovirus, intranasal infection, macrophages, mononuclear phagocyte, mouse cytomegalovirus, viral assembly compartment, viral pathogenesis, virus entry

Editor Felicia Goodrum, University of Arizona

Address correspondence to Berislav Lisnić, berislav.lisnic@medri.uniri.hr.

Received 26 May 2021
Accepted 22 October 2021
Accepted manuscript posted online 27 October 2021
Published 26 January 2022

Human cytomegalovirus (HCMV), a betaherpesvirus widespread in human populations, usually causes asymptomatic infections in immunocompetent individuals resulting in the establishment of lifelong latency in the host organism with occasional reactivations. However, in immunodeficient patients, such as transplant recipients, patients with AIDS or cancer, HCMV may cause multi-organ disease and is a significant cause of morbidity and mortality (1, 2). Moreover, a congenital HCMV infection can cause considerable and often permanent neurological damage (3). Due to its broad cell tropism, the virus quickly spreads throughout the body, infecting numerous tissues and organs, resulting in various clinical manifestations (4, 5). HCMV enters the cell by fusion with the host cell membrane, a process facilitated by the viral envelope glycoprotein complexes, of which gB, gM/gN, and two variants of gH/gL complexes, trimeric and pentameric, have been studied the most (6, 7). Targeting viral envelope glycoproteins necessary for entry into target cells is a promising approach for developing vaccines (8, 9). However, despite decades of effort, no vaccine or effective therapy against HCMV has yet been approved.

Cytomegaloviruses (CMVs) have dedicated a significant portion of their genomes toward evasion of nearly all arms of the immune response (10–12). Among numerous immune cell types targeted and evaded by the CMVs, the role of mononuclear phagocytes (MNPs), like macrophages and dendritic cells, is very challenging to study. One of the difficulties arises from the fact that MNPs are a highly heterogeneous cell type present in almost every tissue, and the cell markers used to distinguish MNPs subpopulations are often either lacking or controversial (13). Furthermore, MNPs are permissive for CMV infection and are thus important contributing factors not only for the control of the virus but also for its spread (14–16). Finally, MNPs are critical mediators of the immune response and inducers of both innate and adaptive immunity (17).

Another layer of complexity in HCMV research is the species-specificity of HCMV, which can infect only humans. Fortunately, several animal CMVs exist, with murine CMV (MCMV) infection being the most widely utilized model to study CMV pathogenesis (18). Virion and genome composition, the pattern of gene expression, cell entry mechanisms, tissue tropism, and systemic organ pathology are all shared between MCMV and HCMV (19, 20). Both viruses utilize highly functionally and structurally similar glycoproteins for cell entry: gB, gH, gL, gO, gM, and gN (7). HCMV-encoded chemokine UL128, a part of the pentamer complex, also has its homolog in MCMV – MCK-2 chemokine, which forms gH/gL/MCK-2 entry complex (21).

Although complete sequences of CMVs genomes have been known for decades, not all predicted ORFs have assigned functions. Additionally, with the advent of high-throughput analyses, it has become increasingly apparent that transcriptomes and proteomes of herpesviruses are more complex than their genomic maps might suggest (22–28). A comprehensive understanding of various viral transcriptional and protein products and their interaction with the host cell is a prerequisite for developing new therapies and vaccines. We were among the first to utilize RNASeq to analyze the MCMV transcriptome and combined it with cDNA analysis (22) to reveal a remarkable complexity of the MCMV transcriptome and discover several highly expressed regions of the MCMV genome with unknown function, one of which was the M116 locus.

We thus set out to investigate the *M116* gene region, hypothesizing that such a highly expressed genomic region likely has an important function for the virus. M116 ORF, a positional homolog of HCMV UL116, was previously predicted to encode a serine-alanine-rich glycoprotein (19). Recently, HCMV *UL116* and rat CMV (RCMV) homolog *ORF116* were shown to encode glycoproteins important for infectivity (29–32), with UL116 being additionally characterized as a chaperone controlling gH-based complex levels on virions (30, 32). In this study, we have performed a detailed molecular dissection of the *M116* gene region, characterized two M116-encoded transcripts, and experimentally detected and characterized protein M116.1 (M116.1p) for the first time. Our study revealed that M116.1p, UL116, and R116 proteins share several characteristics: all are expressed with late kinetics, N-glycosylated, and localize to the same subcellular

compartment (29–32). In addition, both M116.1p and UL116 proteins interact with MCMV and HCMV gH, respectively, demonstrating yet again that MCMV is an excellent model for studying various aspects of HCMV biology. Furthermore, we show that M116.1p is necessary for the efficient infection of MNPs and its deletion from the CMV genome has an impact on the virus spread *in vivo* in organs rich in MNPs like the spleen and in organs where MNPs are known to be necessary for the spread of the virus. Together, this characterization of M116.1p reveals new insight into the contribution of M116.1p and MNPs to viral pathogenesis. In addition, ΔM116-MCMV, as well as novel α-M116 monoclonal antibody (MAb) generated and characterized in this study, could prove as valuable new tools for studying CMV pathogenesis in a relevant animal model.

RESULTS

Transcriptional analysis of the MCMV M116 gene locus. Molecular profiling of the MCMV and host transcriptomes led to the identification of the M116 locus as one of the most highly transcribed yet uncharacterized genomic regions of the MCMV genome during lytic infection of primary and immortalized mouse fibroblasts (22, 23). According to the early annotations of the MCMV genome, the M116 locus contains a single, uninterrupted, 1.9 kb-long ORF (Fig. 1A) (19). However, using several different approaches, we have later shown that the M116 locus might encode at least two different transcripts: a more abundant, shorter ~1600 nt transcript and a less abundant, longer ~3500 nt transcript, hypothesized to initiate in the neighboring m117 ORF (22). To perform a more detailed transcriptional analysis of the M116 gene locus and determine more precisely the numbers and boundaries of the transcripts originating in this transcriptionally very active region of the MCMV genome, we first performed a Northern blot analysis using total RNA isolated from MEFs after 48 h of infection (hpi) with WT-MCMV. Following denaturing gel-electrophoresis and transfer, membrane-immobilized RNA was probed separately with DIG-labeled, strand-specific, single-stranded RNA probes complementary to transcripts originating either within the m117 (Northern Probe M117 – NP-M117), M116 (NP-M116), or M115 (NP-M115) ORFs (Fig. 1A). As shown in the upper middle panel in Fig. 1B and consistent with our previous results (22), we have detected a larger, ~3500 nt viral transcript and a smaller, ~1600 nt viral transcript using probe NP-M116, which is complementary to any RNA molecule transcribed using the first 260 nucleotides of the M116 ORF as a template. Interestingly, we did not detect any signal on the membrane incubated with the riboprobe NP-M117, which can hybridize to transcripts encompassing 250 nucleotides near the 3′ end of the m117 ORF (Fig. 1A and B upper right). Lack of signal when using riboprobe NP-M117 suggests that larger transcript detected with probe NP-M116 extends over the M115 and M114 ORFs and that, in contrast to previous predictions (22), neither of the two transcripts detected with probe NP-M116 originate within the m117 ORF. Further evidence that the ~3500 nt transcript detected with probe NP-M116 extends over the M115 and M114 ORF was obtained using the riboprobes NP-M115 (Fig. 1B, upper left), NP-M115b (Fig. 1A and B, bottom left), and NP-M114 (Fig. 1A and B, lower right), which detected the same ~3500 nt signal at late phase of infection as the probe NP-M116 (black arrowhead). In accordance with these results and to clearly convey the extent of the two transcripts encompassing the M116 locus, the longer ~3500 nt transcript was named M116-M114 (Fig. 1B, black arrowhead), and the shorter transcript was named M116 (Fig. 1B, white arrowhead). In addition, and consistent with our previous cDNA analysis (22) and RACE results described below, using probes NP-M115, NP-M115b, and NP-M114, we have also detected an additional signal corresponding to a transcript that comprises ORFs M114 and M115 of the MCMV genome (Fig. 1B, black arrow). Furthermore, Northern blot analysis revealed the absence of the M116 transcript and truncation of the longer M116-M114 transcript in cells infected with either ΔM116-MCMV or $\Delta M116^{R}$-MCMV (Fig. 1B, upper middle). In addition, no changes in the

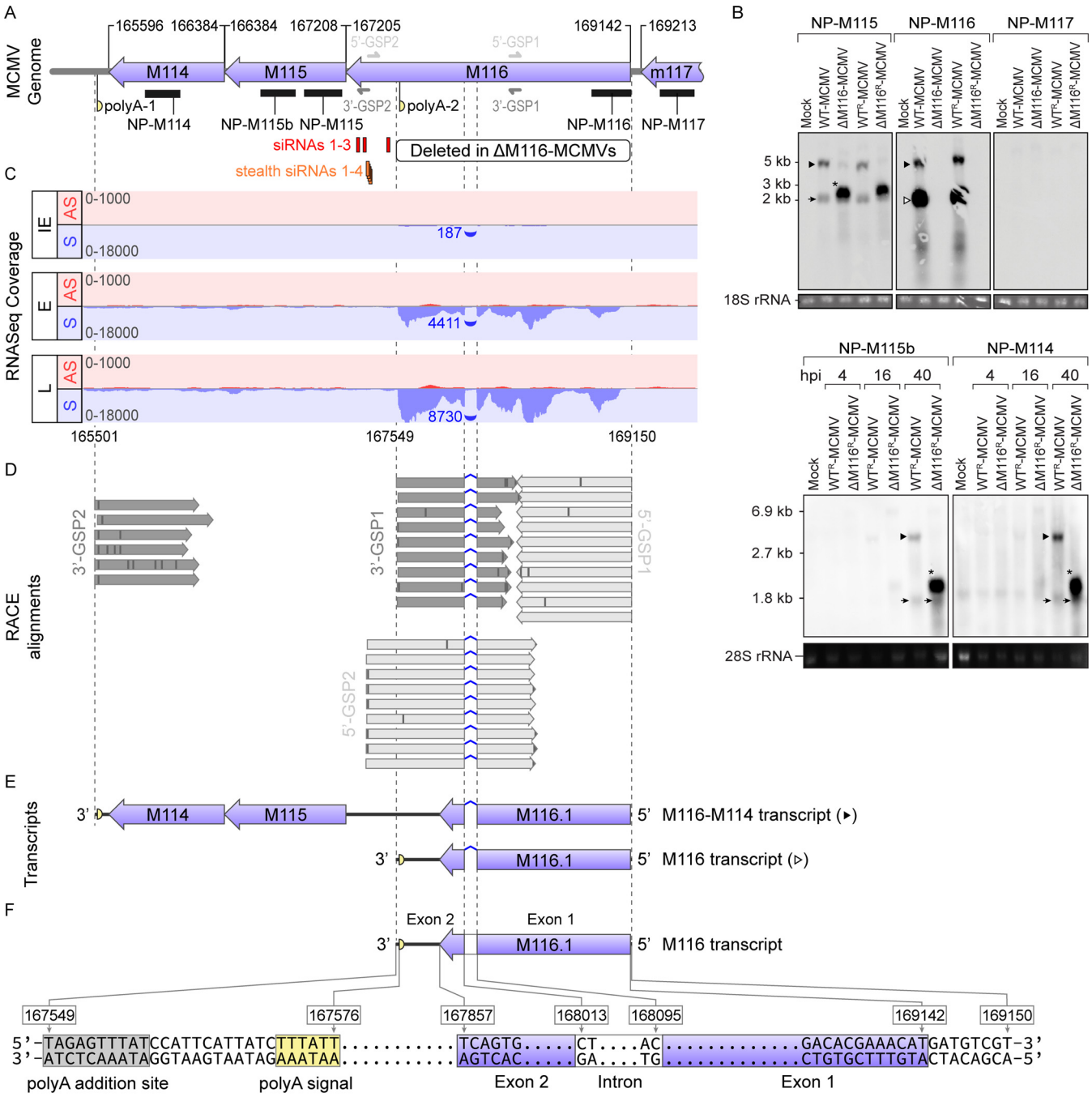

FIG 1 The M116 locus encodes two 5′ coterminal transcripts. (A) A segment of the MCMV genome, showing the location of the M116 and neighboring ORFs according to initial MCMV genome annotation. The first and last base pair of each ORF, excluding STOP codons, are indicated by numbers above the arrows representing each ORF. Black bars denote the transcript segments that are complementary to the strand-specific riboprobes NP-M117, NP-M116, NP-M115, NP-M115b, and NP-M114 used for Northern blotting. Small half arrows denote the binding sites for the 5′-GSP1, 5′-GSP2, 3′-GSP1, and 3′-GSP2 primers used for RACE analysis, the white rectangle represents the region that was deleted from the genome in the ΔM116-MCMVs, while the red and orange rectangles denote regions targeted by siRNAs. Putative polyA sites are labeled with yellow semicircles. (B) Northern blot analysis of the M116 region from total RNA isolated at 48 hpi and hybridized with strand-specific riboprobes NP-M117, NP-M116, and NP-M115 (top), and from total RNA isolated at 4, 16, and 40 hpi and hybridized with strand-specific riboprobes NP-M115b, NP-M114 (bottom). White arrowhead corresponds to M116 and black arrowhead to M116-M114 transcripts. Asterisk denotes truncated M116-M114 transcript and black arrows M115-M114 transcript. (C) RNASeq profile of the M116 region. Raw sequencing libraries representing each phase of the infection (IE, E, and L) were normalized by subsampling each to 15M reads before mapping to the MCMV genome and visualization in IGV. Within and around the M116 ORF, the sense (S) coverage profile is shown in light blue, and the antisense (AS) read coverage profile in light red. The numbers of spliced reads spanning the splice junction within M116 are shown near the arcs connecting the corresponding donor and acceptor splice sites. (D) RACE PCR and alignment of the spliced 5′- and 3′-RACE PCR products to the MCMV genome. 5′-RACE sequences are shown in light gray, 3′-RACE sequences in dark gray, and disagreements with the MCMV genome sequence with thin black lines within each RACE PCR sequence. (E) Schematic representation of the length and boundaries of the M116 and M116-M114 transcripts showing M116.1 ORF exon 1 and exon 2. The white and black arrowheads correspond to the associated transcripts in Fig. 1B. (F) Overview of the M116 transcript. The putative protein-coding region is highlighted with purple, polyA signal with a yellow semicircle, intron with white, and putative polyA addition site with a gray rectangle. Genomic coordinates of relevant features are shown above the map of the M116 sequence. Each dashed line connects the identical location of the MCMV genome on Fig. 1A, C to F.

transcription levels or kinetics of the neighboring M115-M114 transcript were observed between WT^R-MCMV and $\Delta M116^R$-MCMV viruses (Fig. 1B).

Next, to gain a more detailed view of the changes that occur in the transcriptional profile of the M114-M116 region during infection, we have analyzed RNASeq reads from our previous RNASeq experiment (reference 33 and unpublished data), in which total RNA was collected at several time points during IE, E, and L phase of infection, and sequenced using a strand-specific protocol. As shown in Fig. 1C and consistent with the results of other studies (22, 34, 35), this analysis confirmed that the M116 locus was transcriptionally most active at later phases of the infection and revealed numerous spliced RNASeq reads spanning a previously reported intron (22) that extends from base pair 168013 to base pair 168095 within the M116 ORF. These M116 intron coordinates are slightly different from those published in Fig. S3 of our previous work (22), where we have inadvertently reported the imprecise intron coordinates (168016-168090) and size due to the manner in which MegaBLAST performs gapped alignments.

The RNASeq analysis also did not reveal any additional splice sites within the M116 ORF, and the high transcriptional activity of the M116 locus in the sense direction was not accompanied by a significant anti-sense transcription, in line with our previously published Northern blot data (22). Indeed, less than 0.45% of all reads restricted to the M116 region at later time points were mapped in the anti-sense orientation, most likely representing a spurious anti-sense signal (Fig. 1C) (36–39).

Finally, using RNA isolated from infected MEFs at 48 hpi, we have set out to determine the M116 and M116-M114 transcripts' boundaries. First, we have performed 5′ and 3′ rapid amplification of cDNA ends (RACE) using gene-specific primers 5′-GSP1 (for 5′-RACE) and 3′-GSP1 (for 3′-RACE), which can anneal to a sequence upstream of the M116 intron splice sites, as shown in Fig. 1A. Both 5′-RACE PCR and 3′-RACE PCRs generated a single PCR product with an estimated size between 800 and 900 bp. The 5′-RACE and 3′-RACE PCR products were then cloned and sequenced, and obtained sequences aligned to the MCMV genome sequence (NC_004065.1). As shown in Fig. 1D to F, all 5′-RACE PCR products consisted of sequences extending from the binding site of the 5′-GSP1 primer up to the T:A base pair at coordinate 169150 of the MCMV genome, located proximal to the M116 ORF. Since the 5′-GSP1 primer could bind both M116-M114 and M116 cDNA, the absence of two distinct 5′-RACE PCR products led us to conclude that the M116-M114 and M116 represent two 5′-coterminal, or very nearly coterminal, RNAs that are transcribed from the same transcriptional start site located at or near nucleotide 169150 of the MCMV genome, ~8 bp upstream of the M116 ORF sequence (Fig. 1D to F). Moreover, analysis of the 3′ RACE PCR products revealed that they contained sequences extending downstream from the 3′-GSP1 binding site over the putative polyA site 2 at coordinates 167571 to 167576; the longest reaching the T:A base pair at coordinate 167549 of the MCMV genome (Fig. 1D to F). Furthermore, nine out of 11 sequenced 3′-RACE PCR products lacked sequences corresponding to the intron within the M116 ORF and contained a long stretch of T:A basepairs 12–21 bp downstream of the polyA site 2, suggesting the existence of a polyA tail in the 3′-end of the M116 transcript. These results indicate that the M116 intron is associated with the M116 primary transcript encoded by nucleotides 167549 to 169150 of the MCMV genome, which after processing results in a spliced, polyadenylated, two-exon M116 mRNA (Fig. 1D to F).

To identify the 3′ boundary of the longer M116-M114 transcript, we have performed a second 3′-RACE PCR using the 3′-GSP2 primer. As shown in Fig. 1A, we have chosen the annealing location of the 3′-GSP2 primer in such a way as to ensure that the PCR products of the second 3′-RACE PCR do not exceed recommended size (3 kb) and that the primer binds only the cDNA of the M116-M114 transcript and not the cDNA of M116 or, for example, another RNA molecule whose transcription might be initiated near the 5′-end of the M115 ORF. Consistent with the Northern analysis results, the second 3′-RACE reaction resulted in a PCR product slightly smaller than 2000 bp, confirming that the M116-M114 transcript extends over the M114-M115

ORFs. The sequencing and alignment of the second 3′-RACE PCR products further uncovered that the last base pair used as a template for synthesis of the M116-M114 transcript is located downstream of the M114 ORF, near the coordinate 165501 of the MCMV genome (Fig. 1D to F). Furthermore, the presence of a long stretch of T:A base pairs immediately downstream of another putative polyA signal (polyA-1) in this second set of 3′-RACE PCR products indicated that the mature M116-M114 mRNA is also polyadenylated. Subsequently, to determine whether the longer M116-M114 transcript undergoes splicing at the same splice junctions as the shorter M116 transcript, we have performed an additional 5′-RACE PCR using the 5′-GSP2 primer. Similar to the 3′-GSP2, the 5′-GSP2 primer binds only the cDNA of the longer M116-M114 and not the cDNA of the shorter M116 transcript (Fig. 1A). As shown in Fig. 1D, nine out of 10 sequenced second 5′-RACE PCR products lacked sequences corresponding to the intron within the M116-M114 transcript indicating that, in addition to the shorter M116 transcript, the M116 intron sequence spanning base pairs 168013–168095 within the M116 locus, is also spliced out of the longer M116-M114 primary transcript. In summary, the MCMV gene locus encodes two late, 5′-coterminal, spliced, and polyadenylated ~3500 nt (M116-M114) and ~1600 nt (M116) transcripts.

Initial annotation of the MCMV genome predicted that the 1.9 kb M116 ORF encodes a 645 AA protein with a presumed molecular mass of 66.1 kDa (19). However, splicing of the 83 bp M116 intron changes the reading frame downstream from the 349th codon (encoding Gln) and creates a novel UGA STOP codon immediately after the 400th codon (encoding His) within the initially predicted M116 sequence. These changes result in the creation of a novel, two-exon spliced ORF within the mature M116 and M116-M114 transcripts (Fig. 1E and F), which we named M116.1. To initiate a systematic analysis of the role of the putative M116.1 protein (M116.1p) encoded by the newly identified spliced M116.1 ORF present in M116 and M116-M114 transcripts, we have deleted the sequence encoding the most highly expressed portion of the initially predicted M116 ORF (19), including the entire M116.1 ORF (Fig. 1A, white rectangle), from the genomes of two different MCMV strains. The first MCMV strain, referred to herein as WT-MCMV, is a pSM2fr-derived MCMV strain (VR-1399 [40, 41]) shown to be biologically equivalent to the Smith strain of MCMV. The second MCMV strain, referred to as WT^{R}-MCMV (repaired MCMV), is a pSM3fr-MCK-2fl-cl.3.3-derived virus with a reversion of the naturally occurring frameshift mutation within the ORF encoding MCMV chemokine homolog MCK-2 (42). Consequently, corresponding deletion mutants derived from these viruses were named ΔM116-MCMV and ΔM116^{R}-MCMV, respectively.

M116 transcript encodes a conserved protein expressed with late kinetics. To facilitate the characterization of a putative M116.1p encoded by the spliced M116.1 ORF present in the M116 and M116-M114 transcripts, we have expressed the recombinant, His-tagged M116.1p using IPTG-inducible expression system in *E. coli* and used the purified protein for the production of monoclonal antibodies (MAbs) against the M116.1p. According to bioinformatic analysis, M116.1p is an N-glycosylated, strongly acidic (pI = 4.31) protein with a high abundance of serine, alanine, and proline, and a predicted molecular mass of 40.2 kDa (Fig. 2A). Based on the high content of Ser, Ala, and Pro, which comprise 45.1% of all amino acids in the M116.1p (Fig. 2A), as well as low pI value and many negatively charged residues, we anticipated that the M116.1p might display anomalous mobility during SDS-PAGE and migrate much more slowly than expected from its calculated molecular mass (43–47). Indeed, a single, highly abundant protein species of an apparent molecular mass of ~70 kDa was produced following IPTG induction of *E. coli* cells carrying recombinant, spliced M116.1p sequence (Fig. 2B, first panel). The induced protein was purified (Fig. 2B, second panel), verified for the presence of the His-tag (Fig. 2B, third panel), and used as an antigen for producing MAbs against M116.1p. The obtained α-M116 MAb specifically recognized the ~70 kDa recombinant M116.1p (Fig. 2B, fourth panel) and an ~70 kDa protein in the lysates of WT-MCMV infected MEFs (Fig. 2C). As can be seen in Fig. 2C, no bands

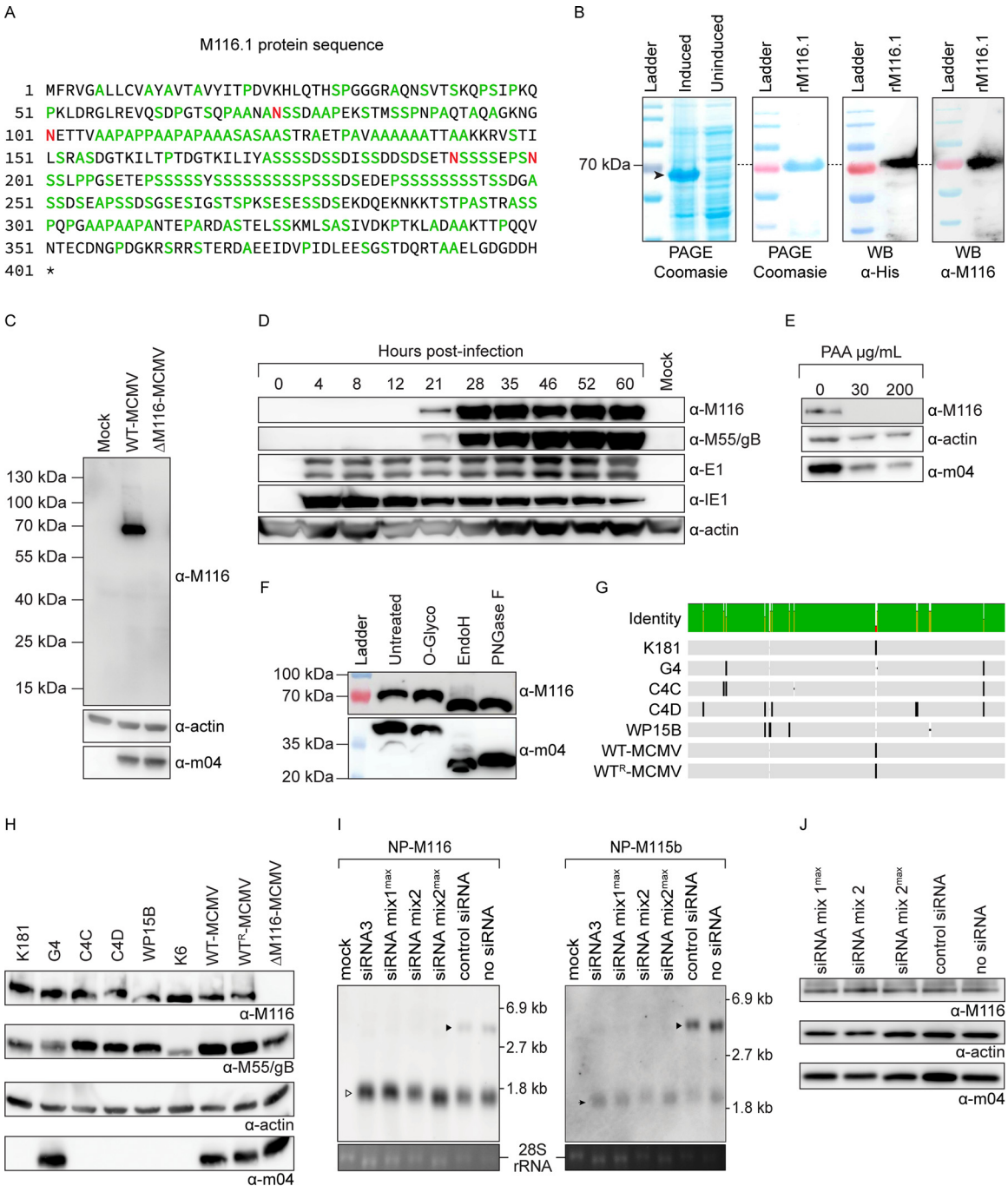

FIG 2 M116 transcript encodes a conserved protein expressed with late kinetics. (A) Amino acid sequence showing a high abundance of serine, alanine, and proline residues (green), which comprise 45.1% of all amino acids, in the M116.1p. Predicted N-glycosylation sites are shown in red. (B) Expression, purification, and anomalous migration of the recombinant M116.1p (rM116.1p). A single band, corresponding to a protein with an apparent molecular mass of ~70 kDa (black arrowhead), was detected in the lysates of induced *E. coli* cultures transformed with rM116.1 ORF (first panel). Coomassie stain of purified rM116.1p used for the generation of α-M116 MAb (second panel). WB of purified rM116.1p detected with anti-His (third panel) or α-M116 MAb (rightmost panel). Contrast of the whole image has been slightly increased for better clarity. (C) Specificity of α-M116 MAb. Lysates of MEFs infected with WT-MCMV or ΔM116-MCMV were subjected to Western blot analysis using the α-M116 MAb. The MAb binds to the ~70kDa protein present only in lysates of WT-MCMV infected MEFs. Note that the virally encoded M116.1p also displays aberrant migration. (D) Kinetics of M116.1p expression. Total proteins were isolated at indicated hpi from MEFs infected with WT-MCMV and analyzed by WB using MAbs against M116.1p, and immediate early (IE), early (E), and late (M55/gB) viral proteins. Actin was used as a loading control. Lane labeled "Mock" represents a protein sample isolated from mock-infected MEFs at 48 hpi. (E) PAA treatment of MEFs infected with WT-MCMV inhibits M116.1p expression. Immediately following infection, PAA was added to MEFs at the indicated concentrations. At 48 hpi, total proteins were isolated from infected cells and analyzed by WB using α-M116 MAb. (F) Analysis of M116.1p glycosylation at 48 hpi. Lysates of WT-MCMV infected MEFs were treated with O-glycosidase, Endoglycosidase H, or PNGase F. Only treatment with

(Continued on next page)

were detected in the lysates of either mock-infected cells or cells infected with MCMV lacking the M116.1p coding sequence (ΔM116-MCMV), confirming the specificity of our α-M116 MAb and demonstrating that the virally encoded M116.1p also displays aberrant migration during SDS-PAGE. Occasionally, a very faint band between the 100 and 130 kDa markers was also visible in the lysates of the cells infected with WT-MCMV (e.g., Fig. 2C). We hypothesize that this band, which was not always detectable even with prolonged exposure times, corresponds to a rare protein species arising from the translation of the unprocessed (unspliced) M116 and M116-M114 transcripts. We next collected cellular lysates at multiple time points postinfection and compared the pattern of M116.1p expression with the expression kinetics of immediate early (IE1), early (E1), and late (M55/gB) MCMV proteins. M116.1p was detected in the lysates of WT-MCMV infected cells from 21 h postinfection (hpi) onward and exhibited the expression kinetics identical to the late MCMV protein M55/gB (Fig. 2D). Furthermore, the expression of M116.1p, but not of the early protein m04, was entirely abolished by phosphonoacetic acid (PAA) treatment (Fig. 2E) of MCMV-infected cells, establishing the M116.1p as a late MCMV gene/protein.

Analysis of the amino acid sequence using SPRINT-Gly (48) led to the prediction of zero potential O-glycosylation sites and four potential N-glycosylation sites at amino acid residues 74, 101, 192, and 200 within the M116.1p with probabilities of 0.998, 0.999, 0.980, and 0.979, respectively (Fig. 2A). Since the virally encoded M116.1p migrated during SDS-PAGE at approximately the same rate as the recombinant, His-tagged M116.1p produced in prokaryotic cells (Fig. 2B and C), we did not expect that the M116.1p might be extensively glycosylated. Indeed, following endoglycosidase H (Endo H), Peptide N Glycosidase F (PNGase F), or O-glycosidase (O-Glyco) treatment of total protein samples isolated from WT-MCMV infected MEFs at 48 hpi, we observed a slight reduction in apparent molecular mass of the M116.1p only in PNGase or Endo H treated samples. Both enzymes had a similar effect and reduced the apparent molecular mass of M116.1p by only a few kDa (Fig. 2F), suggesting that the M116.1p is a lightly glycosylated glycoprotein containing N-linked oligomannose or hybrid types of N-glycans. In these experiments, m04, a known viral N-linked glycoprotein, served as a control of infection and control for Endo H and PNGase F activity (49). Further sequence analysis revealed that the novel M116.1p glycoprotein is highly conserved across various laboratory strains and field isolates of MCMV (Fig. 2G). Indeed, similar to gB, we were able to detect the M116.1p in lysates of MEFs infected with laboratory MCMV strains and field isolates available in our laboratory (Fig. 2H), while the apparent absence of protein bands corresponding to m04 in K181, C4C, C4D, WP15B, and K6 MCMV strains was consistent with a high variability of m04 sequence reported previously (50).

Considering that the M116.1p might originate from both the M116 and M116-M114 transcripts, we employed specific siRNAs to selectively target and neutralize the longer M116-M114 transcript RNA (locations of the siRNA binding sites are shown in Fig. 1A). Northern blot analysis of total RNA isolated from lysates of MCMV-infected primary MEFs treated with M116-M114-specific siRNAs confirmed successful silencing of the M116-M114 transcript, whereas the levels of the smaller M116 and M115-M114 transcripts remained the same as in the control cells, which were either treated with control siRNAs or left untreated (Fig. 2I). Furthermore, despite the successful knockdown of the longer M116-M114 transcript, levels of the M116.1p in cells treated with M116-M114-specific siRNAs, control siRNAs, and untreated cells remained the same (Fig. 2J). These results

FIG 2 Legend (Continued)
Endoglycosidase H or PNGase F led to a slight reduction in the apparent molecular mass of M116.1p, indicating that the M116.1p is lightly glycosylated N-linked glycoprotein. (G) The amino acid sequence of M116.1p is conserved among different strains, and field isolates of MCMV. Black lines denote polymorphisms. Alignment was made in Geneious software v7.1.9 (Biomatter) using MUSCLE algorithm. (H) M116.1p is detected in lysates of MEFs infected with all analyzed MCMV strains and field isolates 48 hpi. Expression of the viral proteins gB- and m04, and the expression of the cellular protein actin, were used as infection and loading controls, respectively. (I-J) siRNA knockdown of M116-M114 transcript by two different siRNA mixes and individual siRNA has no effect on M116 nor M115-M114 transcripts (I) nor amount of M116.1p (J) indicating that M116.1p is dominantly translated from M116 transcript. MEFs transfected with mix of siRNAs targeting M116-M114 transcript and infected 6h later with WT^R-gH-HA-MCMV were lysed 40 hpi and subjected to Western and Northern blot analyses.

indicate that the 70 kDa M116.1p represents a major protein form encoded by the *M116* gene locus and translated predominantly from the shorter M116 transcript.

Next, using BLAST (51), as well as SnapGene implementation of MUSCLE sequence alignment algorithm (52), we have compared the amino acid sequence of M116.1p and its positional and presumed functional homologs in human (UL116) and rat CMV (R116), along with previously detected M116.1 in EastMCMV (53). Neither algorithm was able to find significant sequence similarities between M116.1p, UL116, and R116. On the other hand, the amino acid sequences of EastMCMV M116.1 and MCMV M116.1p shared substantial homology of over 98% (Fig. 3A). Interestingly, the N-terminus of the M116.1 protein from EastMCMV is shorter by 84 amino acids, which might reflect biological differences between EastMCMV and Smith-derived MCMVs. Nonetheless, these alignment results prompted us to investigate whether the ATG codon present at the beginning of the M116.1p coding sequence (base pairs 169142–169144 of the MCMV genome, Fig. 1F) acts as a true initiator codon for translation of the M116.1p. To that end, we have generated an M116-STOP-MCMV mutant, in which point-mutations have been introduced at the N-terminus of the M116.1p so that 9th and 12th amino acid codons were mutated into stop codons (Fig. 3B). Cells infected with M116-STOP-MCMV expressed both M116 and M116-M114 transcripts (Fig. 3C and D) but contained no detectable amounts of M116.1p (Fig. 3E). Interestingly, the introduction of these point mutations had a moderate negative impact on the expression levels or stability of the M116 and M116-M114 transcripts at 40 hpi (Fig. 3C and D), which is why we limited the use of this mutant to the minority of experiments. Nonetheless, the absence of the M116.1p in cells infected with M116-STOP MCMV confirms that the protein-coding sequence of the M116.1p begins at position 169142 of the MCMV genome.

M116.1p localizes to the virion assembly compartment (VAC). Having established that the M116.1p is expressed in cultured MEFs *in vitro*, we set out to determine whether M116.1p is expressed in the infected organs *in vivo*. To that end, we infected BALB/c mice with WT-MCMV and ΔM116-MCMV, collected the organs at 4 dpi, and probed the neighboring sections of the livers for the expression of M116.1p, as well as IE1, a widely used marker for MCMV infection. As shown in Fig. 4A, M116.1p can be detected throughout the cytoplasm of infected hepatocytes, but it tends to accumulate in the perinuclear region. As expected, the nuclei of the M116.1p-positive cells also tended to stain positive for IE1, while no M116.1p staining was detected in organs of ΔM116-MCMV infected animals, where the infected cells were readily identifiable by the presence of inclusion bodies typical for the MCMV infection (Fig. 4A, rightmost panel, black arrowhead).

Predominant signal in the perinuclear region observed in the infected hepatocytes suggested that the M116.1p might preferentially accumulate in the specialized compartment within infected cells and prompted us to examine its subcellular localization more thoroughly. To that end, we first performed confocal microscopy analysis of fibroblasts infected *in vitro* with WT-MCMV, MCMV lacking Fc-receptor protein m138 (Δm138-MCMV), as well as ΔM116-MCMV. Similar to infected hepatocytes (Fig. 4A), we could observe preferential localization of the M116.1p in the perinuclear region of the primary BALB/c MEFs infected with WT-MCMV (Fig. 4B, first panel) and the complete absence of the nonspecific or viral Fc-mediated binding of the primary α-M116 or secondary MAb (Fig. 4B, second, third, and fifth panel). During microscopic examinations of infected cells, cell rounding, a common hallmark of MCMV infection (54), often makes it difficult to determine whether a particular protein is associated with the plasma membrane. Therefore, following infection with WT-MCMV and ΔM116-MCMV, we have stained permeabilized or non-permeabilized primary BALB/c fibroblasts with the α-M116 MAb and used flow cytometry to investigate whether the M116.1p is present on the cell surface. As shown in Fig. 4C, in contrast to permeabilized fibroblasts, we did not observe any shift in the fluorescence intensity after staining non-permeabilized, WT-MCMV infected fibroblasts with the α-M116 MAb, indicating that the M116.1p is not present on the surface of infected cells.

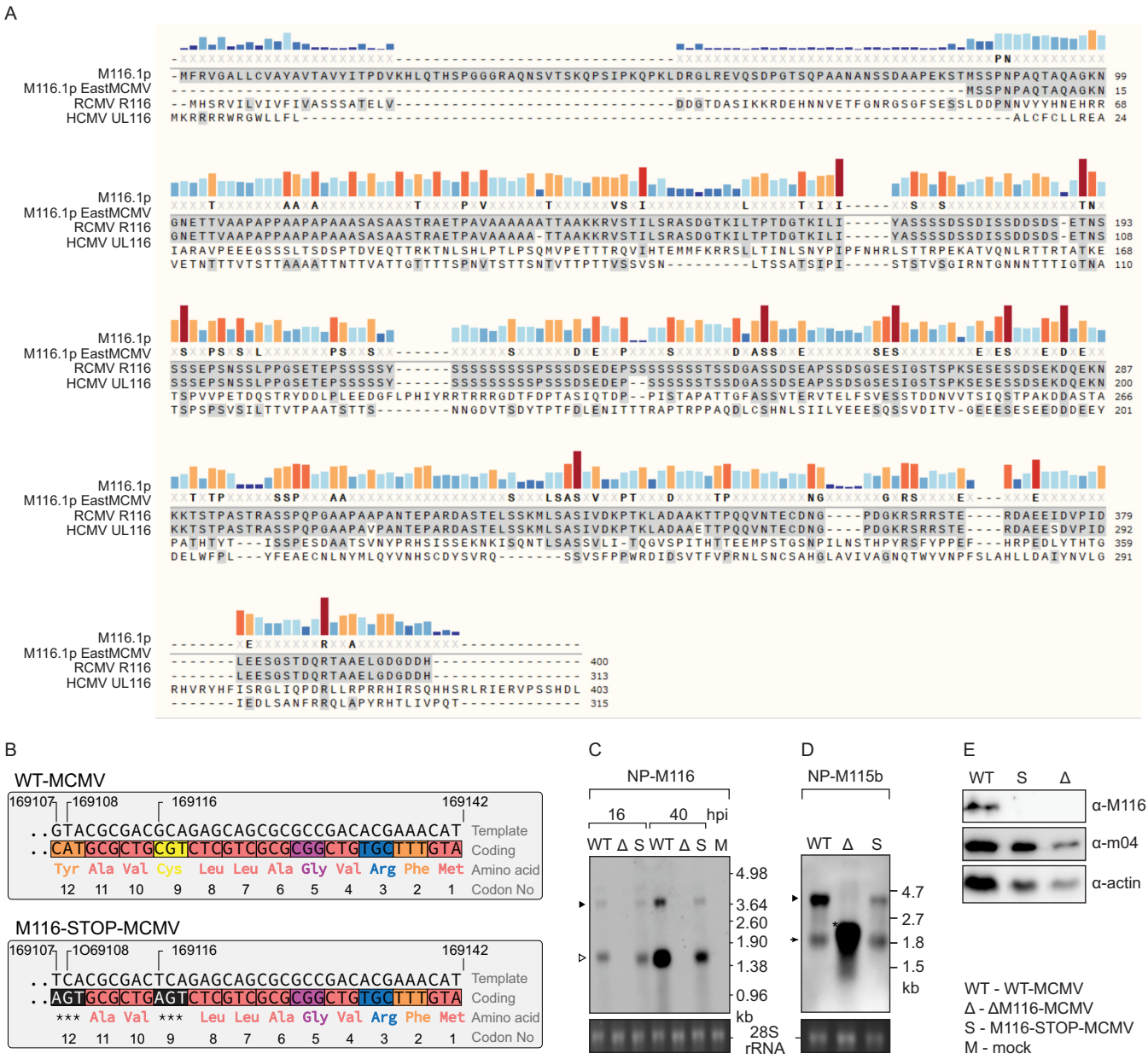

FIG 3 Comparison of amino acid sequences of M116.1p with its EastMCMV, HCMV, and RCMV homologs and analysis of M116.1p translation start site. (A) Protein sequence alignment of M116.1p from MCMV, EastMCMV, R116, and UL116 using MUSCLE aligner in SnapGene software. M116.1p from CMV has been used as reference sequence. The bars above demonstrate amino acid similarity (higher bar and more red—higher similarity) and consensus amino acids are written in bold. (B) Nucleotide and amino acid sequence of the first 12 codons of the M116.1p in WT-MCMV and M116-STOP-MCMV. Point-mutations have been introduced so that 9th and 12th amino acid codons of M116.1p were mutated into stop codons. (C-D) Northern blot analysis of M116 gene region using strand-specific riboprobes NP-M116 and NP-M115b. MEFs were infected with indicated viruses and collected at 16 and 40 hpi, total RNA was isolated and hybridized with NP-M116 and NP-M115b probes. Sequence changes introduced in M116-STOP-MCMV resulted in altered amounts of M116-M114 transcripts but not of M115-M114 transcript at late time points. (E) Western blot on the lysates of MEFs infected with indicated viruses and collected at 48 hpi, detected with indicated MAbs. No M116.1p band is visible in M116-STOP MCMV infected MEFs.

Since the localization of the M116.1p in the perinuclear region resembled the localization of other viral proteins that localize to the virus assembly compartment (VAC) (55), we have performed confocal microscopy colocalization analysis using MAbs against M116.1p and cellular markers Rab6, Rab10, and Rab31 to determine the subcellular localization of M116.1p more precisely. Localization of M116.1p clearly overlapped with Rab6, a marker of the trans-Golgi that builds the outer ring of the VAC (oVAC), but not with Rab10, a marker of early endosome (EE) – endosomal recycling compartment (ERC) interface that localizes to the inner VAC (Fig. 4D). A portion of the M116.1p was also found in distinct membranous

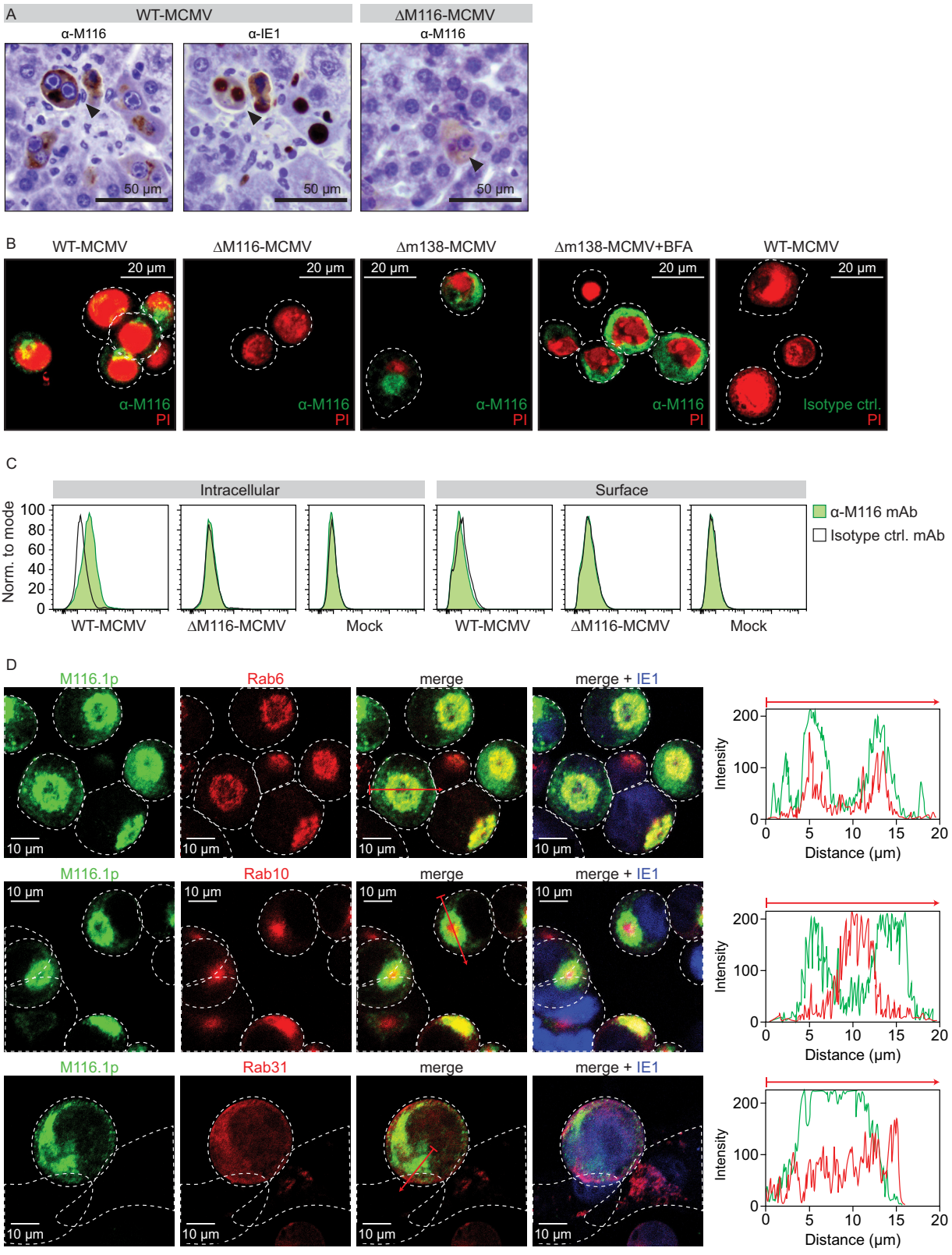

FIG 4 M116.1p localizes to the oVAC. (A) M116.1p is detected in the liver of WT-MCMV-infected BALB/c mice *in vivo* at 4 dpi. Expression of M116.1p and IE1 was analyzed by immunohistochemistry in the neighboring sections. Control staining of mice infected with ΔM116-MCMV shows no unspecific M116.1p staining. Black arrowheads—enlarged infected cells with typical inclusion bodies. Contrast and brightness have been slightly modified on the entire image. (B) M116.1p localizes in the perinuclear region. MEFs infected with WT-MCMV, ΔM116-MCMV, or Δm138-MCMV were stained at 30 hpi with α-M116, isotype control MAbs, or propidium iodide (PI) to stain nuclei. (C) M116.1p cannot be

(Continued on next page)

structures outside the outer ring of the VAC (Fig. 4D), suggesting that it also accumulates in the peripheral membranous structures of the secretory pathway. Significant overlap with Rab31 (Fig. 4D), a small GTPase that associates with tubulo-vesicular carriers that bud from the TGN and post-TGN compartments (56), and is not a component of VAC, indicates the post-Golgi secretory trafficking of M116.1p. Altogether, these data indicate that a considerable proportion of M116.1p is directed to the oVAC area, an intracellular site that accumulates viral structural glycoproteins.

M116.1p interacts with the gH in the oVAC but is not detectable in gradient-purified MCMV virions. Localization of the M116.1p to the oVAC, together with results of a previous study reporting the presence of M116 peptides in the MS spectra of MCMV virions (57), raised the possibility that the M116.1p might be a structural MCMV protein, similarly to its HCMV and RCMV homologs UL116 and R116, respectively (29, 31). To investigate such a possibility, we have first analyzed the lysates of the WT-MCMV virions, prepared using standard sucrose cushion purification procedure, by SDS-PAGE and Western blotting (18), and have detected a band corresponding to the M116.1p (Fig. 5A, left lane). However, having in mind the presence of M116.1p in the post-Golgi secretory trafficking system (Fig. 4D), as well as the results of studies that show that routine virus preparations may be contaminated with extracellular vesicles (i.e., exosomes), containing both viral and host proteins (reviewed in references 58 and 59), we decided to investigate the apparent presence of M116.1p in MCMV stocks in more detail. In agreement with localization analysis and the presence of a Sec/SPI-type signal peptide on its N-terminus (60), we have first established that M116.1p can be detected in supernatants of infected fibroblasts. Moreover, treatment of cells with Brefeldin A (BFA), a commonly used protein secretion inhibitor (61), let to the accumulation of the M116.1p inside the infected cells and its complete absence from the supernatants (Fig. 4B and 5C). Highly abundant cytoplasmic viral protein m04 was used as a control to show that supernatants have not been contaminated with contents of lysed infected cells (Fig. 5C). Having established that MCMV-infected cells secrete M116.1p, we next analyzed WT-MCMV stocks for the presence of the established exosomal marker CD63 (62). As presumed, strong, CD63-positive staining was detected in lysates of infected cells as well as sucrose-cushion purified virions (Fig. 5B), suggesting that the M116.1p signal shown in Fig. 5A, instead of being indicative of the M116.1p presence in MCMV particles, might instead be attributable to the contamination of WT-MCMV stocks with exosomes containing M116.1p. We next took advantage of the fact that the mature CMV particles have different buoyant densities from the extracellular vesicles produced in infected fibroblasts (63) and have used sorbitol density gradient (SG) centrifugation to purify MCMV stocks further. M116.1p was not detectable, while a strong signal corresponding to M55/gB, a known component of MCMV virions, was clearly visible in the SG purified MCMV virions (Fig. 5A, right lane). Moreover, sorbitol-gradient purified virus preparation retained infectivity and had a high virus titer, as demonstrated by a standard plaque-forming assay (data not shown). Taken together, these results indicate that the M116.1p is not incorporated into infectious MCMV-particles, at least not at levels detectable in Western blot with α-M116 MAb, but is instead secreted, possibly within exosomes, from MCMV infected cells.

Even though the M116.1p was present in the peripheral membranous structures of the secretory pathway and consequently secreted, a significant portion of intracellular M116.1p was nonetheless localized to oVAC (Fig. 4D). HCMV UL116 also localizes to VAC and interacts with gH (29, 30, 32). We thus investigated whether M116.1p and gH

FIG 4 Legend (Continued)
detected on the surface of infected cells. Flow-cytometric profiles of intracellular and surface expression of M116.1p at 30 hpi are presented by green histograms and isotype control-stained cells by transparent histograms. (D) M116.1p co-localizes with the marker of the outer virion assembly compartment (oVAC). Balb 3T3 fibroblasts infected with Δm138-MCMV were fixed 48 hpi. Intracellular distribution of M116.1p, IE1 (infection marker), cellular markers Rab6 (trans-Golgi), Rab10 (EE/ERC), and Rab31 (peripheral compartments) was analyzed by triple immunofluorescence and confocal microscopy. Dashed lines indicate cell borders. The fluorescence intensity profiles (measured along the red arrows) for colocalization of Rab6, Rab10, and Rab31 with M116.1p are shown on the right, with M116.1p depicted in green and cellular markers shown in red.

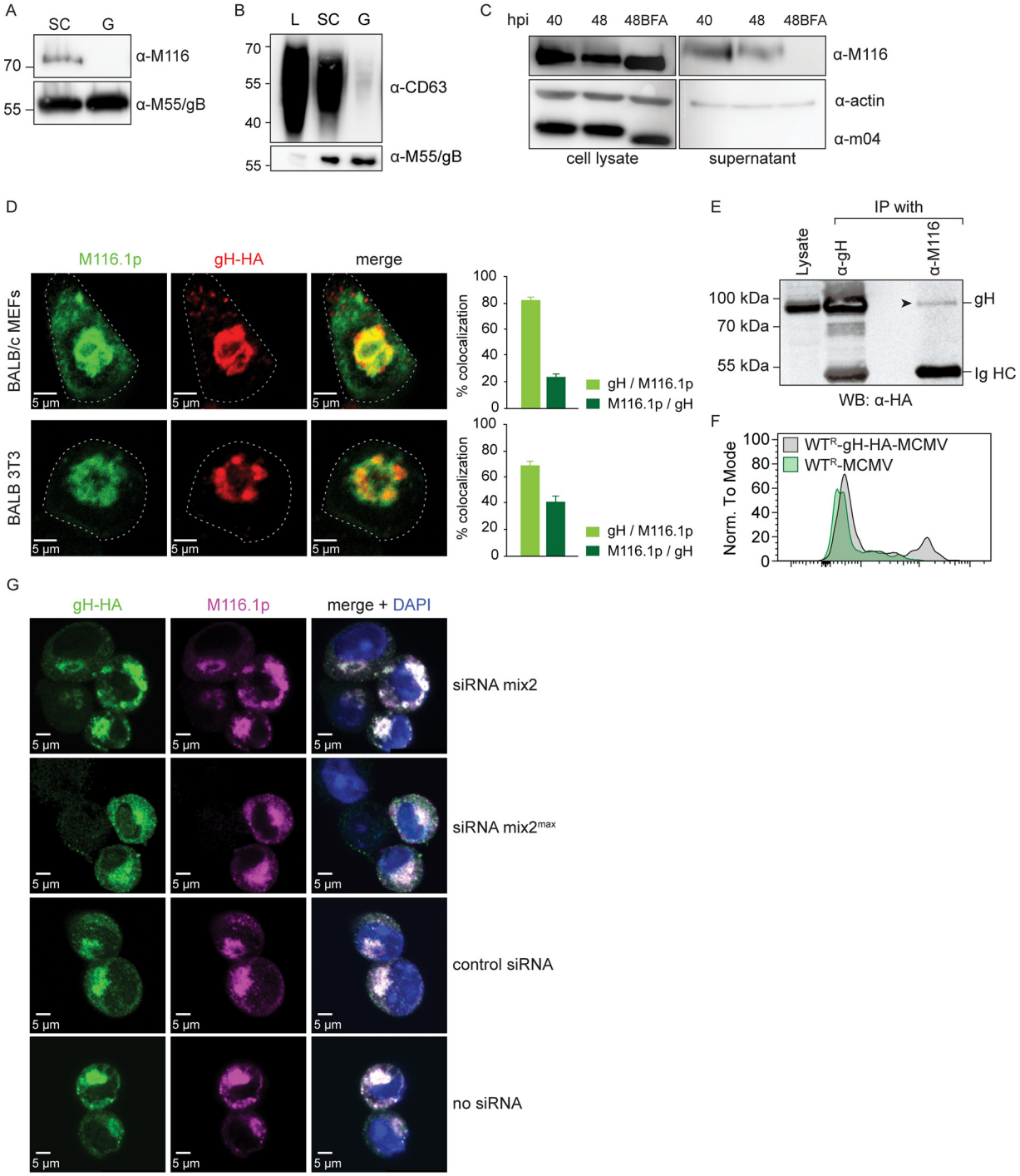

FIG 5 M116.1p is not present in the MCMV virions but interacts with gH in the oVAC. (A-B) WB analysis of virus stocks obtained by either pelleting viral particles through a low-density sucrose cushion (SC) or by sorbitol gradient purification (G). The proteins from the lysed virus stocks were separated by SDS-PAGE and immunoblotted with MAbs against viral proteins gB/M55 and M116.1p (A) or exosome marker CD63 (B). L – WT-MCMV infected MEFs lysate. (C) M116.1p is detected both in lysates and supernatants of infected MEFs, while treatment with BFA blocks its secretion. Supernatants and lysates of MEFs infected with WT-MCMV were harvested at indicated hpi and immunoblotted with α-M116 MAb. Marked samples were treated with BFA (3 μg/ml) from 40 to 48 hpi. MCMV m04 and cellular actin served as infection and loading controls, respectively. (D) Colocalization analysis of M116.1p and gH. MEFs or Balb 3T3 fibroblasts infected with WT^R-gH-HA-MCMV were fixed 48 hpi and stained with α-M116 and α-HA (RM305) MAbs. Dashed lines indicate cell borders. (E) M116.1p immunoprecipitates with gH. Lysates of WT^R-gH-HA-MCMV infected primary BALB/c MEFs were co-incubated with α-M116 or α-gH MAbs, and protein-MAb complexes subsequently isolated using protein G Sepharose beads. Bead eluates were separated by PAGE and following transfer membranes incubated with α-HA (3F10) MAb, revealing that gH co-immunoprecipitates with α-M116.1p (arrowhead). (F) Proximity ligation assay demonstrating an interaction between M116.1p and gH. Primary BALB/c MEFs were infected with WT^R-gH-HA-MCMV (gray) or WT^R-MCMV (green), collected and stained 48 hpi with α-M116, α-HA, and secondary MAbs. (G) siRNA-mediated silencing of M116-M114 transcript had no effect on the localization of M116.1p. MEFs transfected with mix of siRNAs targeting M116-M114 transcript and infected 6h later with WT^R-gH-HA-MCMV were fixed 40 hpi and stained with α-M116 and α-HA (3F10) MAbs and DAPI to stain nuclei.

also co-localize in the VAC. Regardless of whether we used primary BALB/c MEFs or immortalized Balb 3T3 cells, M116.1p and gH clearly co-localized (Fig. 5D) in a ring-shaped structure identified as oVAC in Fig. 4D. We then performed co-immunoprecipitation utilizing recombinant MCMV with HA-tagged gH (WT^R-gH-HA-MCMV) to enable the detection of gH in Western blot. M116.1p was immunoprecipitated with α-M116 MAb, while gH was immunoprecipitated using mouse α-gH MAb (clone 8D122A). The immunoprecipitate was analyzed on Western blot with MAb against HA (for gH, clone 3F10) (Fig. 5E). gH co-precipitated with M116.1p, indicating the interaction between these proteins. To further confirm the interaction, we have performed a proximity ligation assay on WT^R-MCMV or WT^R-gH-HA-MCMV-infected primary BALB/c MEFs using α-M116 and α-HA (clone F-7) MAbs. Signal in the proximity ligation assay is only generated if the two molecules are located at approximately 40 nm or closer (64, 65). As shown in Fig. 5F, we could detect a clear interaction signal between M116.1p and HA-tagged gH in WT^R-gH-HA-MCMV-infected MEFs but no signal in the negative control (WT^R-MCMV infected MEFs). Finally, siRNA silencing of the M116-M114 transcript did not affect either detectability of M116.1p, as already demonstrated in Western blot in Fig. 2J, or its co-localization with gH (Fig. 5G). These results collectively indicate that, like HCMV UL116, M116.1p interacts with gH in the VAC, where both could act as chaperones for stabilizing gH (32).

M116.1p is required for efficient virus growth in mononuclear phagocytes. It is well established that various protein complexes with gH play a role in determining virus tropism and providing means of entry both for human and murine CMVs (21, 66–68). To investigate whether M116.1p is required for MCMV replication in different cell types *in vitro*, we have first performed a multi-step growth curve analysis of WT-MCMV and ΔM116-MCMV in highly permissive cells, primary BALB/c-derived MEFs (Fig. 6A). ΔM116-MCMV displayed no significant growth defects compared to WT-MCMV, although the viral titers of ΔM116-MCMV were slightly lower than of WT-MCMV. Since primary MEFs preparations often contain a proportion of CD11b positive cells (69, 70), usually mononuclear phagocytes (MNPs), we next investigated MCMV growth in immortalized bone-marrow-derived macrophages (iBMDMs). We observed a substantial impairment of infectious virus production in iBMDMs, with the peak titers being more than 100-fold lower for ΔM116-MCMV than the WT-MCMV virus (Fig. 6B). Additionally, ΔM116-MCMV was attenuated in primary MNPs derived from bone-marrow cells from either BALB/c or C57BL6 mice, both in the cells representing the floating and the adherent fractions (Fig. 6C to E). Although both fractions comprise a heterogenous population of MNPs, dendritic cells, and macrophages, it is considered that the floating fraction is enriched in dendritic cells, while the adherent fraction is enriched in macrophages (71, 72). Furthermore, the same defect in the *in vitro* growth in MNPs was observed for the M116-STOP-MCMV (Fig. 6F and G). We thus concluded that M116.1p is an essential factor necessary for efficient virus growth in dendritic cells and macrophages.

Since MCMV-encoded chemokine MCK-2 plays an important role in the infection of macrophages (21), we next investigated whether the absence of functional *MCK-2* gene influences attenuation of viruses lacking M116.1p. For this reason, primary MNPs were infected with both variants of WT-MCMV and ΔM116-MCMV viruses: MCK-2 deficient (WT-MCMV and ΔM116-MCMV) and "repaired" variants (WT^R-MCMV and ΔM116^R-MCMV) where MCK-2 is functional (42). As shown in Fig. 6H, both viruses lacking M116.1p displayed attenuated growth kinetics, indicating that the absence of M116.1p induces *in vitro* growth defects in MNPs irrespective of the viral MCK-2 functionality.

M116.1p is required for efficient viral spread *in vivo*. Our *in vitro* analysis revealed that M116.1p is required for efficient infectious virus production in MNPs. Since MNPs play important but complex roles in the spread and immune control of the virus, where the outcome often depends on the infection route (10, 73–80), we compared virus titers between WT-MCMV and ΔM116-MCMV in different organs following infection by several routes.

To study the role of M116.1p in systemic MCMV infection, BALB/c mice were infected intravenously (i.v.) with 2×10^5 PFU of the indicated viruses, and viral titers in spleen, lungs, liver, and salivary glands (SG) were determined on days 1.5, 4, 7, and 14 pi (Fig. 7A). In most of the tested time points, there were no significant differences between the viral titers of

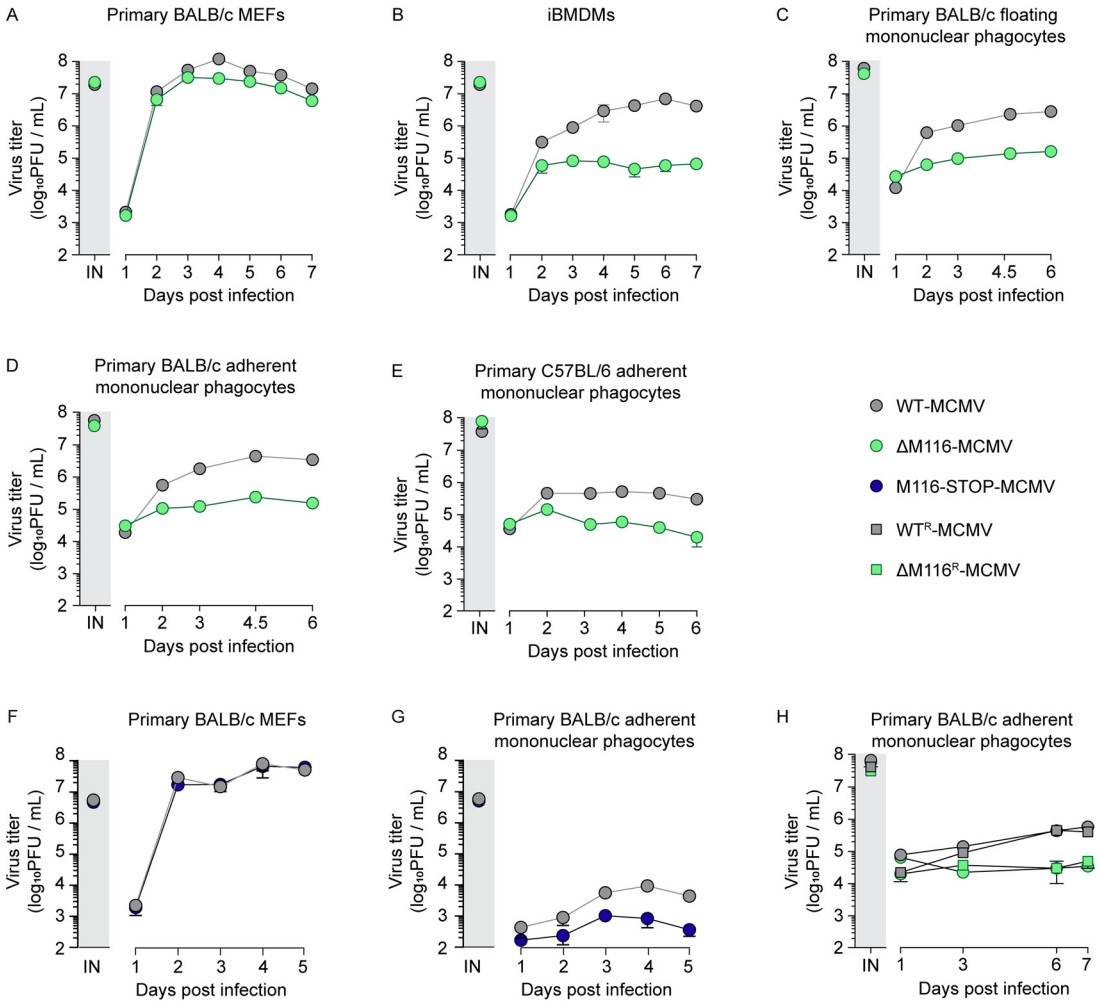

FIG 6 M116.1p is required for virus growth in mononuclear phagocytes. (A, F) Primary BALB/c MEFs, (B) iBMDMs, (C) primary BALB/c floating MNPs, (D, G, H) primary BALB/c adherent MNPs and (E) primary C57BL6 adherent MNPs were infected with the indicated viruses at an MOI of 0.1 PFU/cell. Supernatants of infected cells were collected at indicated dpi and titers determined by plaque assay. Data points represent means ± SEM of triplicate (A-E, G) or duplicate (F, H) samples. All experiments have been performed 2 or more times.

the WT^R-MCMV and ΔM116^R-MCMV viruses, suggesting that deletion of M116.1 ORF from the genome of MCMV does not have a major impact on the spread of the virus following systemic infection. One exception is the spleen at 4 dpi where the MCMV lacking M116.1p displayed approximately 1 log attenuation.

We next investigated the impact of M116 deletion when the virus spreads from peripheral sites via the footpad (f.p.) and intranasal (i.n.) route. The f.p. infection with either WT^R-MCMV or ΔM116^R-MCMV yielded a similar amount of virus in the draining, popliteal lymph nodes (PLNs) at 3 dpi and in SG 14 dpi, indicating that M116.1p is not required for efficient spread following f.p. infection (Fig. 7B).

Upon i.n. inoculation, the route that most accurately mimics the natural infection, we observed attenuation of ΔM116^R-MCMV in lungs and SG at 14 dpi (Fig. 7C). These results indicate that the absence of M116.1p diminishes the ability of MCMV to successfully disseminate to and from organs with high concentrations of MNPs, like the spleen, or organs in which MNPs play an important role in virus dissemination, like the SG.

DISCUSSION

In this study, we characterized the properties and function of *M116*, previously poorly described but highly transcribed MCMV ORF. M116 was originally annotated by

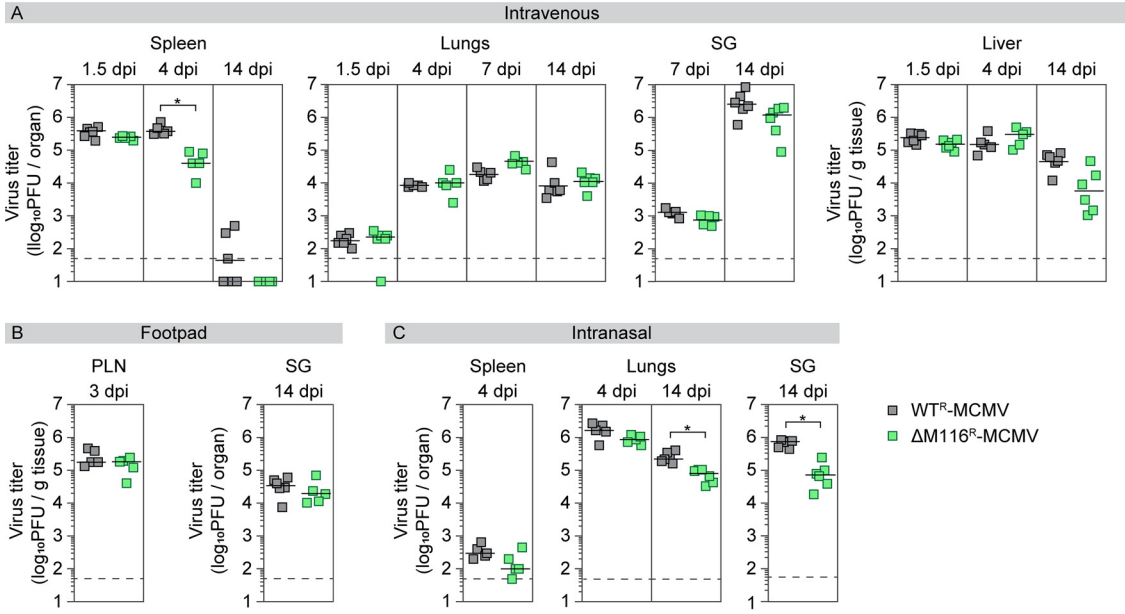

FIG 7 M116.1p is required for efficient viral spread *in vivo*. BALB/c mice were infected with 2×10^5 PFU/mouse of WT^R-MCMV or ΔM116^R-MCMV either intravenously (A), intra-footpad (B), or intranasally (C). Viral titers were determined in the indicated organs of individual mice (squares) at the indicated time points. Horizontal bars show the median values and dotted line detection limit (50 PFU/organ). PLN, popliteal lymph node; SG, salivary glands. Statistical significance was calculated by Mann-Whitney two-tailed test. $^*P < 0.01$.

Rawlinson and colleagues and postulated to encode serine-alanine-rich glycoprotein, a positional homolog of HCMV *UL116* (19). Although the transcriptional profile of *UL116* has not been studied in detail, recent works indicate that it encodes at least one protein important for virus tropism (29, 30, 32). We thus set out to investigate M116 under the rationale a) that it should have an important function due to its high expression levels; b) that it might have a similar role to UL116; and c) that due to the similarities between HCMV and MCMV, the obtained results could expand our understanding of HCMV UL116. Studies of the pathogenesis of MCMV in mice have so far provided invaluable insight into the pathology of CMVs that could then be extrapolated for HCMV (81). A homolog of an HCMV gene influencing tropism and spread allows us to study its role in the context of various infection routes.

We have performed a detailed characterization of the transcriptional product of the *M116* locus and defined the boundaries of two 5′ co-terminal transcripts, M116 and M116-M114, discovered in our previous study (22). Using RACE and RNASeq, we have further demonstrated that the large majority of both M116 and M116-M114 primary transcripts undergo splicing and that the transcriptional profile of the M116 locus is similar to R116, a recently characterized RCMV-encoded M116 homolog that also gives rise to two transcripts and contains a small intron (31). Even though the large majority of M116 and M116-M114 RNA molecules were spliced, we could still detect a minor proportion of cDNA/RNASeq sequencing reads aligning to the M116 intron. These rare unspliced variants that may represent unprocessed M116 and M116-M114 primary transcripts that have yet to undergo splicing. Alternatively, these rare unspliced variants might represent a minor subpopulation of transcripts that have evaded the splicing and in which intron has been retained due to, for example, the high abundance of M116 and other transcripts that oversaturate cellular splicing machinery (82).

To facilitate further analyses of potential protein products encoded by the *M116* gene region, we have generated and characterized a novel MAb, α-M116, which detected a late, highly acidic protein M116.1p that contains a few N-linked and no O-linked glycans, unlike R116 and UL116, which are highly N- and O-glycosylated. In addition, we have occasionally observed a pale band between 100 and 130 kDa using the

α-M116 MAb that could correspond to the M116 protein encoded by the initially predicted M116 ORF arising from the occasional unspliced transcript. The dominant protein species, 70 kDa M116.1p, is predominantly translated from the more abundant M116 transcript, as demonstrated by our siRNA experiments in which no changes in M116.1p levels or in co-localization were detected upon successful silencing of the M116-M114 transcript.

M116.1p is highly conserved between various MCMV strains, including the more distantly-related EastMCMV (53), suggesting its importance for the virus, although it shares no obvious nucleotide or amino acid sequence similarities between its homologs, HCMV UL116 and RCMV R116. However, absence of amino acid homology does not exclude functional or structural homology, as already demonstrated for m42 and pUL42 proteins of MCMV and HCMV (83). Our results indicate that M116.1p shares numerous functional properties with UL116 and R116 since all three proteins have been localized to the VAC, where UL116 and M116.1p interact with HCMV and MCMV gH, respectively. Even though UL116 and R116 were found in the virus particles, we did not detect M116.1p in sorbitol gradient-purified virions. Absence of O-glycans in M116.1p could account for its absence in the virions as it was recently demonstrated that herpesviral envelope glycoproteins tend to contain O-glycans (68, 84). Furthermore, the only study proposing that product of M116 ORF is a virion associated protein (57) has only detected two peptides that could have originated from *M116* ORF. Additionally, our data show that the quantity of M116.1p in the purified virus stocks correlates with the quantity of CD63, an exosomal marker. M116.1p was undetectable in gradient-purified stocks with low levels of CD63. Also, we have detected M116.1p in the supernatants of infected cells, suggesting it is either secreted or a component of exosomes, while the studies of UL116 and R116 have not addressed this issue. However, it should be noted that it is also possible that the M116.1p is a component of the mature MCMV virion, albeit in amounts that are below the detection level of our assays.

Although originally considered a component of a new glycoprotein complex (29), recent studies proposed that UL116 acts as a chaperone for gH, supporting the assembly, maturation, and incorporation of gH/gL complexes into virions (30, 32). A potential chaperone whose role is to ensure proper incorporation of envelope glycoproteins does not necessarily have to be a virion protein, as demonstrated for gO and UL148 (68, 84). Instead, it might serve its chaperone function in the virion assembly compartment, preferably in the outer VAC, where other viral envelope glycoproteins are usually located (55), which is precisely the location where we detect M116.1p. Thus, we propose that M116.1p performs an analogous function as a chaperone for MCMV gH.

Glycoprotein complexes formed with gH have a major effect on the herpesvirus entry and, consequently, on the cell tropism (6, 7). Having shown that M116.1p interacts with gH, we investigated *in vitro* and *in vivo* growth of viruses lacking M116.1p. Unlike UL116-null HCMV and RCMV with silenced R116 (30–32), ΔM116-MCMV and M116-STOP-MCMV displayed no significant growth defects compared with WT-MCMV in fibroblasts. However, the deletion of M116.1p led to a marked growth deficit in MNPs. We next compared virus titers in various organs following three different inoculation routes to account for virus exposure to particular cell types and pathway(s) of virus dissemination dictated by the inoculation route (85). Since virally-encoded chemokine MCK-2 also plays a role in MNP attraction and infection (21), viral strains with functional MCK-2 protein were used for *in vivo* studies. We observed no difference in virus growth curves, M116.1p expression, or transcriptional profiles between MCK-2 mutated or repaired virus strains. Similarly to MCMV lacking *M140* gene region that also grows poorly in MNPs (86, 87), ΔM116^{R}-MCMV did not display dramatic attenuation upon systemic infection in the liver, SG, or lungs but was attenuated in the spleen at 4 dpi. Upon systemic infection, the virus quickly reaches the spleen via blood, where it can infect reticular fibroblasts and endothelial cells of the splenic sinusoidal capillaries (74). Unlike lungs, liver, or SG, the spleen contains a high concentration of MNPs surrounding the capillaries that serve to prevent the hematogenous spread of an infectious agent, containing the spread of ΔM116^{R}-MCMV resulting in attenuation at 4 dpi.

Upon i.n. infection, we observed attenuation of ΔM116^R-MCMV in lungs and SG at 14 dpi. Following i.n. infection, MCMV first infects olfactory neurons and the nasal mucosa and then further spreads via dendritic cells to lungs and SG, while infection of the abdominal visceral organs is less prominent (77, 78, 88). Attenuation of ΔM116^R-MCMV in the SG at 14 dpi speaks in favor of MNPs as vehicles for virus transmission from the nasal mucosa. Intranasal inoculation also results in lung infection, with lung epithelium and alveolar macrophages being the first cells to be infected (89–92). Thus, attenuation of ΔM116^R-MCMV in the lungs only at a later time point goes in line with the alveolar epithelial cells being the major virus-producing cell in the lung early after infection, as already proposed by Yunis et al.(93).

Footpad-inoculated (f.p.) MCMV first reaches the popliteal lymph nodes (PLNs), primarily infecting CD169$^+$ subcapsular sinus macrophages (SSM) (76), which act as main shields preventing virus spread but poorly support the infection. In line with that, we observed no difference between WT-MCMV and ΔM116^R-MCMV titers in the PLNs. We could also observe no difference in virus titers at SG at 14 dpi following f.p. inoculation speaking against patrolling monocytes as virus dissemination vehicles from PLNs to distal sites (94).

The role of MNPs in the CMV infection is challenging to study as they play two opposing roles: on the one hand, they are considered to be an important reservoir of latent virus and vehicles for virus spread while also being the first responders to infection along with NK cells (10, 11) and important mediators of adaptive immunity as antigen-presenting cells. It is thus not surprising that CMVs have evolved multiple genes that modulate the antiviral activity of MNPs; M27, M35, M36, M45, M78, m139, and M140 have all been initially identified as determinants for tropism of macrophages since the mutants lacking these nonessential regions are attenuated in macrophages, but not in fibroblasts *in vitro*. M27 protein acts as a modulator that disrupts IFNAR signaling (95); M36 and M45 proteins have been identified as inhibitors of apoptotic and necroptotic cell death responses in macrophages, respectively (96–98); M78 facilitates the accumulation of immediate early viral mRNA and is considered to stimulate SG infection by protecting infected dendritic cells against CD4$^+$ cell engagement (93, 99) and m139 targets DDX3 to curtail the production of interferon by macrophages (100), while M140 is required for efficient production of mature capsids in macrophages (86). Additionally, MCMV proteins M35, which modulates type I IFN signaling in macrophages (101), and the MCK-2 (21), are also required for efficient MCMV replication in macrophages. Furthermore, MNPs are a large and diverse group composed of numerous types that are often difficult to distinguish functionally and phenotypically (13) and even harder to extract *ex vivo* for *in vitro* studies. Thus, M116.1p is not just yet another arrow in CMV's quiver directed at manipulating this important immune cell population. Instead, mutant viruses lacking MNP-evasive genes could also be considered as tools for teasing out complex roles of MNPs in virus spread and dissemination.

Finally, our α-M116 MAb has proved to be a valuable tool for the detection of M116.1p in every technique we have tested (Western blot, flow cytometry, immunohistochemistry, confocal microscopy, PLA, immunoprecipitation). As M116.1p is quite abundant and clearly visible in different microscopy techniques, we propose it could be a useful marker of both late infected cells and as a virus marker for oVAC.

MATERIALS AND METHODS

Cells. Primary BALB/c mouse embryonic fibroblasts (MEFs) were prepared as previously described (18). Balb 3T3 immortalized fibroblasts were obtained from American Type Culture Collection (ATCC; BALB/3T3 clone A31, ATCC CCL-163). Immortalized bone-marrow-derived macrophages (iBMDM) cell line NR-9456 derived from C57BL6/J mice can be obtained from BEI Resources, NIAID NIH. Both primary BALB/c MEFs and immortalized cell lines were cultivated in DMEM supplemented with either 3% or 10% FCS, respectively.

To generate primary mononuclear phagocytes (MNPs), bone-marrow cells from BALB/c or C57BL6 mice were isolated from femur and tibia. The cells were then cultured at the concentration of 1×10^6 cells/ml in Not TC-Treated Petri dishes (Corning, 430597) in RPMI supplemented with 10% FCS complemented with the supernatant of J558 hybridoma cell line (10-20%, depending on the batch) as a source of granulocyte-macrophage colony-stimulating factor (GM-CSF) (18). On days 3 and 6, additional media

were added (the same volume as when seeded). On day 7, floating and adherent fractions of MNPs were collected separately and used in the subsequent experiments. Following infection, MNPs were cultivated in RPMI supplemented with 10% FCS.

Viruses. WT-MCMV is the bacterial artificial chromosome (BAC)-derived MCMV strain pSM3fr (C3X), shown to be biologically equivalent to the Smith strain of MCMV (VR-1399 [40]). WT^R-MCMV or "repaired" MCMV refers to pSM3fr-MCK-2fl-cl.3.3-derived virus with a reversion of the frameshift mutation within the ORF encoding MCMV chemokine homolog MCK-2 (42). Generation of WT-MCMV mutant with a deletion of *m138* ORF (Δm138-MCMV) and WT^R-MCMV mutant with C-terminally HA-tagged gH (WT^R-gH-HA-MCMV) was previously described (21, 102). WT MCMV strains K181 (GenBank accession no. AM886412), G4 (GenBank accession no. EU579859), c4C (GenBank accession no. HE610453), c4D (GenBank accession no. HE610456), K6 (103), and WP15B (GenBank accession no. EU579860 [104, 105]) were a kind gift from A. Redwood (University of Western Australia, Perth, Western Australia, Australia).

ΔM116-MCMV and $\Delta M116^R$-MCMV were constructed according to the previously published procedure (106) on two different bacterial artificial chromosomes (BACs) containing the desired MCMV genome (MCMV-BAC); WT-MCMV or WT^R-MCMV. In short, a disruption cassette containing kanamycin resistance gene (Kan^R) and I-SceI restriction site was amplified in a two-step PCR using primers dM116-F-long (5′-gagtttttccccgtca ccccatcaactatttaacctctcggacacgctcgccgtgagggcacgacatcccagtatacactccgctagc-3′), dM116-R-long (5′-tggtgac gacctgcgtgcggaacgcggcgctaggagaagacacagactcggatgtcgtgccctcacggcgagcgtgtccgagaggttaaagctctgcca-gtgtt acaacc-3′), Kan-R-short (5′- taatgctctgccagtgttac-3′), and dM116-F-Short (5′- gagtttttccccgtcacc-3′) using plasmid pEP-SaphA as a template. *Escherichia coli* strain GS1783 containing MCMV-BACs were then transformed with the amplified DNA fragment, resulting in the deletion of the nucleotides 167548 to 169142 of the MCMV genome, corresponding to the nucleotides encoding the M116 transcript, following homologous recombination. The kanamycin-carrying cassette was then removed from kanamycin-resisting clones by inducible endonuclease I-SceI, resulting in the precise deletion of M116.1 ORF in MCMV-BAC. To generate the M116-STOP-MCMV, we have introduced point mutations resulting in STOP codons at the place of 9th and 12th amino acid of M116.1p. A disruption cassette containing kanamycin resistance gene (KanR) and I-SceI restriction site was amplified in a two-step PCR with primers M116-STOP-For (5′-tcgccgtgagggcacgacatcatgtttcgtgtcggc gcgctgctct**ga**gtcgcgt**ga**gccaggatgacgacgataagtag-3′), M116-STOP-Rev (5′-gaatgagtctggaggtgcttgacatccggtg ttatgtatacggccgtcacggc**tc**acgcgac**t**cagagcagcgcgccgacacgaaacatgcaaccaattaaccaattctg-3′), M116-STOP-Short-For (5′-tcgccgtgagggcacgacat-3′), and Kan-Univ-Rev (5′-gccagtgttacaaccaattaacc-3′) using plasmid pEPkanS as a template (the locations of point mutations are bolded and STOP codons underlined). *Escherichia coli* strain GS1783 containing WT-MCMV BAC (pSM3fr) were then transformed with the amplified DNA fragment, following the removal of kanamycin-carrying cassette. The integrity of the mutated BACs was verified by restriction enzyme analysis and by sequencing of the modified region. Infectious viral particles were then reconstituted by transfection of purified BAC DNA into primary BALB/c MEFs using XtremeGene9 transfection reagent (Roche) according to the manufacturer's instructions. After the appearance of viral plaques, the infective supernatants were used for further propagation.

Preparation of MCMV stocks. Virus stocks were prepared on primary BALB/c MEFs as described previously (18) by ultracentrifugation and pelleting through a low-density sucrose solution to reduce aggregation. Where highly purified virions were necessary, the above-mentioned virus preparations were purified on sorbitol gradient. Virions were first enriched by ultracentrifugation of the cell culture supernatants as described. The pellet was then resuspended in 1 ml of DMEM supplemented with 3% FCS and the suspension was overlaid on a continuous 20% to 70% (wt/vol) sorbitol gradient in PBS and centrifuged in a swing-bucket rotor at 70 000 × *g* for 60 min at 4°C (Thermo Scientific Sorvall WX Ultra Series centrifuge, Surespin 630 rotor). The virus-containing band was detected by light scattering, collected by aspiration, diluted in PBS, and pelleted by ultracentrifugation at 70 000 × *g* for 60 min at 4°C. Pellet was resuspended in PBS, aliquoted, and frozen at −80°C. Virus titers were determined by a standard plaque-forming assay (18).

Infection of cultured cells with MCMV *in vitro*. For Western blot, flow cytometry, and microscopy analyses, primary BALB/c MEFs were infected with 0.5 PFU/cell, while immortalized Balb 3T3 fibroblasts were infected with 1 PFU/cell. Unless stated differently, infection was performed by co-incubating cell suspension at a concentration of 10^7 cells/ml with the virus for 30 min with occasional agitation at 37°C and in an atmosphere with 5% CO_2, the method equivalent to incubating adherent cell layer for 30 min in a small volume of virus suspension at 37°C and an atmosphere with 5% CO_2, followed by 30 min centrifugation at 800 × *g* (centrifugal enhancement) (107). Following incubation, cells were plated (approximately 0.5 × 10^6 cells in a 6-well plate, or 1–1.5 × 10^6 cells in a 10-cm culture dish) and further incubated at 37°C in a 5% CO_2 humidified atmosphere.

In vitro viral growth was analyzed by infecting cultured cells (MEFs, iBMDM, or primary MNP) with indicated viruses at 0.1 PFU/cell in a suspension as described above. Following incubation, the unbound virus was washed with media, and cells were pelleted 5 min at 500 × *g*. This washing step was repeated 3 times. The cells were plated on a 48-well plate at a concentration of 0.2 × 10^6 cells/well. At indicated dpi, the duplicates or triplicates of the cell-free culture supernatants were collected and stored at −80°C. The amount of extracellular infectious virus present in the culture supernatant was determined by a standard plaque-forming assay (18).

siRNA knock-down of M116-M114 transcript. To selectively knock down the M116-M114 transcript, we have employed siRNA targeting M116-M114 transcript positions (167 326 – 167 523) that should target exclusively M116-M114 transcript and not M116 or M115-M114. Primary BALB/c MEFs (250 000 cells/well) were seeded 1 day before transfection in complete medium without antibiotics in 6-well plates with glass coverslips. The cells were transfected the next day with individual siRNAs at a final concentration of 20 nM or their combination (20 nM each or 20 nM in total) using Lipofectamine RNAiMAX

Reagent (Invitrogen) according to the manufacturer's protocol for forward transfection. Additionally, negative control (scrambled) siRNA (Stealth RNAi siRNA Negative Control Hi GC) has been used. Six h after transfection, the cells were infected with WT^R-gH-HA-MCMV (0,5 PFU/cell with centrifugal enhancement); 24 h after transfection, the medium was replaced with the fresh complete medium with antibiotics; and 46 h after transfection, the glass coverslips were collected for the microscopy analysis as described below, and the remaining cells were lysed in either TRI Reagent (RNA analysis) or RIPA buffer (protein analysis) and subjected to Northern blot and Western blot analyses as described below.

siRNA duplexes used (sense strand): siRNA1 (Eurogentec, 5′- cgacucgcucauuaucgau-3′), siRNA2 (Eurogentec, 5′- gacucagucucucaaacag-3′), siRNA3 (Eurogentec, 5′- gagucugugucuucuccua - 3′), stealth siRNA1 (Invitrogen, 5′- gcgcuagcgacgucgccauauuuaa-3′), stealth siRNA2 (Invitrogen, 5′- gcgacgucgccauauuuaacgacuc - 3′), stealth siRNA3 (Invitrogen, 5′- ucgccauauuuaacgacucgcucau - 3′), and stealth siRNA4 (Invitrogen, 5′- ccauauuuaacgacucgcucauuau - 3′). siRNA mix 1 contained siRNA1, siRNA2, and siRNA3, while the siRNA mix 2 contained stealth siRNA1, stealth siRNA2, stealth siRNA3, and stealth siRNA4. siRNA mix denotes that equal amounts of individual siRNAs were added to a final concentration of 20 pmol/ml of siRNA, while siRNA mix^{max} denotes a mixture containing 20 pmol/ml of each siRNA.

Northern blotting and rapid amplification of cDNA ends (RACE). Primary BALB/c MEFs were mock-infected or infected with either WT-MCMV or ΔM116-MCMV as described above and seeded onto 10 cm tissue culture dishes at an approximate density of 10^6 cells/dish. Following 48 h of incubation, total RNA from MCMV-infected or mock-infected cells was extracted and purified using TRI Reagent (Sigma-Aldrich, Product Number T9424-25ML). The obtained nucleic acid pellet was dissolved by adding RNase-free water containing 20 U of Protector RNase Inhibitor (Sigma-Aldrich, Product Number 3335399001), and obtained RNA suspension was then treated with RNase-free DNase I (New England Biolabs, Catalog Number M0303S) to remove contaminating DNA. Samples of isolated total RNA were stored at −80° C. The stability of purified RNA was verified by incubating small aliquots of each RNA sample at 37°C and 80°C for 2 h and comparing their 28S:18S ratios to the 28S:18S ratio of the original, control sample stored at −80°C on the 2% bleach gel (108). Primer design, generation of RACE ready cDNA, assessment of RNA purity/integrity, RACE reaction, cloning, characterization, sequencing, and analysis of RACE PCR products were performed using the SMARTer RACE 5′/3′ Kit (TaKaRa Bio, Product Number 634858). Gene-specific primers for 5′-RACE (5′-GSP1: 5′- gattacgccaagcttagatggcgcctccgaatccgatgaagcg - 3′ and 5′-GSP2: 5′- gattacgccaagcttaatatggcgacgtcgctagcgcactccg - 3′) and gene-specific primers for 3′ RACE (3′-GSP1: 5′ – gattacgccaagcttcgcttcatcggattcggaggcgccatct - 3′ and 3′-GSP2: 5′ – gattacgccaagctttcgctcattatcgatccgggcctgggcg - 3′) were purchased from biomers.net. Sequences of the 5′-RACE and 3′-RACE products were aligned to the wild-type MCMV genome sequence (NC_004065.1, accessed on 20.08.2020) using SnapGene v5.1.7. Northern blot analysis was performed as described previously (22). Briefly, following the isolation procedure described above, total RNA concentrations in the RNA samples were determined using NanoPhotometer Pearl spectrophotometer (Implen). One microgram of total RNA from each sample was then loaded into the separate well in the formaldehyde-containing agarose gel and separated by denaturing formaldehyde agarose gel electrophoresis. RNA ladders used were Transcript RNA Markers 0.28–6.6 kb (Sigma-Aldrich), RNA Molecular Weight Marker I, DIG-labeled (Sigma-Aldrich), and ssRNA Ladder (New England Biolabs). After electrophoresis, RNA was transferred onto a positively charged nylon membrane (Amersham Hybond $–N^+$) by capillary transfer and immobilized by UV cross-linking (Amersham Biosciences UVC 500 Crosslinker, 800 J/cm2). Subsequently, the membrane was blocked in a brief prehybridization step and then incubated at 68°C overnight in a hybridization solution containing a single-stranded DIG-labeled probe. Following hybridization, probe bound to its cRNA target(s) was detected using the DIG High Prime DNA Labeling and Detection Starter Kit (Merck, Product Number 11585614910), and visualized with an ImageQuant LAS 4000 series imager (GE Healthcare).

Strand-specific Northern blot RNA probes (Probes NP-M117, NP-M116, NP-M115, NP-M115b, and NP-M114, shown in Fig. 1A) were generated in several steps. First, genomic regions spanning nucleotides 169346-169595 (amplicon for NP-M117), 168880-169147 (amplicon for NP-M116), 166924-167181 (amplicon for NP-M115), 166688-166942 (amplicon for NP-M115b), and 165806-166091 (amplicon for NP-M114) of the MCMV genome (NC_004065) were amplified by PCR using primers M117-F (5′- aattaaccctcactaaagggcggtctcgatgtgagtgtt -3) and M117-R (5′- tattgaagaggctcgcggac - 3′) for amplicon M117, primers M116-F (5′-aattaaccctcactaaaggggacgacatcgtgctcttttcg - 3′) and M116-R (5′- acatcatgtttcgtgtcggc - 3′) for amplicon M116, primers M115-F (5′ – taatacgactcactataggagccgtagctcctcttgaacc - 3′) and M115-R (5′- ctgtccacacgtaacctgct - 3′) for amplicon M115, primers M115-b-F (5′ – taatacgactcactataggatcggtcgtgtagttcaaccg – 3′) and M115-b-R (5′ – gttcaagaggagctacggcg – 3′) for amplicon M115b, and primers M114-F (5′ – taatacgactcactataggatccttctctctgctcggaca – 3′) and M114-R (5′ – acaagatccgtaccacgacg – 3′) for amplicon M114, all purchased from biomers.net. Obtained PCR products were then separated by agarose gel electrophoresis and bands corresponding in size to desired DNA fragments excised from the agarose gel and purified using NucleoSpin Gel and PCR Clean-up kit (Macherey-Nagel). A small amount of each purified amplicon was then used as a template for the second PCR using the same primers as above. Each of the second PCR products was then also excised from the agarose gel, column-purified, and used as a template for *in vitro* RNA probe synthesis with the DIG Northern Starter Kit (Sigma-Aldrich, Product Number 12039672910), resulting in five strand-specific RNA probes (NP-M117, NP-M116, NP-M115, NP-M115b, and NP-M114).

RNASeq analysis. Infection of primary BALB/c MEFs for RNASeq was performed as described previously (22, 33). Briefly, MEFs growing in 10-cm cell-culture dishes were infected in two replicates with Smith strain of MCMV at an MOI = 0.3, followed by centrifugal enhancement at 800 × *g* for 30 min. Total RNA from infected MEFs was then isolated at 4, 8, 12, 16, 24, 32, 40, 60, and 80 hpi using TRI Reagent (Sigma-Aldrich, Product Number T9424-25ML), according to manufacturer's instructions. Following RNA

isolation and purification, equal amounts of total RNA isolated from MEFs were then selectively pooled to attain representative RNA samples from different temporal classes of MCMV infection. First, equal amounts of total RNA isolated from 4, 8, and 12 hpi were pooled to obtain an RNA sample representing the immediate early (IE) phase of infection. Equal amounts of total RNA isolated after 16, 24, and 32 hpi were then pooled to obtain an RNA sample from the early (E) phase of the infection, while the equal amounts of total RNA isolated at 40, 60, and 80 hpi were pooled to get an RNA sample characterizing the late (L) phase of MCMV infection. After RNA isolation and pooling, two sequencing libraries for each phase of the infection were prepared using a TruSeq Stranded Total RNA with Ribo-Zero Gold kit (Illumina, San Diego, CA, USA) and sequenced on an Illumina Genome Analyzer IIx to obtain 72 nt, single-ended, strand-specific sequencing reads. Following pre-mapping read quality control, raw reads from the same phase of the infection were first concatenated into a single fastq file, and each fastq file was then subsampled to the same size to containing randomly selected 15M reads. Raw sequencing reads in subsampled fastq files were then mapped to the MCMV genome sequence (NCBI accession number NC_004065) using STAR v (109, 110). Reads aligning to either forward or reverse strand were then separated into two separate bam files using samtools (111), and the read coverage profile for both sense and antisense transcription in the MCMV M114-M116, as well as number of spliced reads spanning the M116 intron, were visualized using IGV (112).

Generation of the α-M116 monoclonal antibody. The sequence encoding the M116 spliced transcript, without the sequence encoding N-terminal Sec/SPI-type signal peptide, was inserted into the bacterial expression plasmid pQE30 (Qiagen) in frame with the N-terminal His tag. The obtained expression plasmid was sequenced to verify the integrity of the M116 sequence and then transformed into the bacteria *E. coli* BL21(DE3) strain (Qiagen). Expression of His-tagged rM116.1p was induced with the addition of isopropyl-β-D-thiogalactoside according to the manufacturer's instructions (QIAExpressionist; Qiagen). The induced protein was purified from bacterial lysates by affinity chromatography on Ni-Sepharose columns. As described previously, purified rM116.1p was then used to immunize BALB/c mice and produce MAbs (113). The specificity of the MAbs produced by several hybridoma clones was first tested against rM116.1p, and irrelevant protein in ELISA and Western blot, followed by Western blotting on mock, WT-MCMV, and ΔM116-MCMV, infected primary MEFs. M116.02 clone was of the highest specificity, was selected for all further analyses, and was affinity-purified on protein G columns.

Western blot analysis. Primary BALB/c MEFs were infected with 0.5 PFU/cell of indicated MCMV as described above. In the indicated experiment, PAA (30 or 200 μg/ml, Sigma-Aldrich) was added immediately following infection or BFA (3 μg/ml, eBioscience) from 40 to 48 hpi. At the indicated times p.i., cell-free supernatants were collected, and cell lysates were prepared using radioimmunoprecipitation assay (RIPA) buffer (25 mM Tris, 150 mM NaCl, 1% Na-deoxycholate, and 0.1% SDS) with the addition of Complete Protease Inhibitor Cocktail (Roche). According to the manufacturer's instructions, the protein concentration was determined with a bicinchoninic acid assay (Pierce BCA Protein assay kit; Thermo Fisher Scientific). Comparable protein amounts mixed with denaturing sample buffer (4% SDS, 10% 2-mercaptoethanol, 20% glycerol, 0,004% bromophenol blue, 0,125M Tris HCl) were separated on 8–10% SDS-polyacrylamide gels in Laemmli buffer on constant voltage. Following separation, proteins were transferred to Amersham Hybond PVDF membranes with 0.45 μm pores (GE Healthcare) using Trans-blot semidry transfer system (Bio-Rad) in Bjerrum Schafer-Nielsen transfer buffer (48 mMTris, 39 mM glycine, and 20% methanol, pH 9.2). Membranes were blocked with 5% nonfat milk in Tris-buffered saline with 1% of Tween 20 (TBST) for ≥30 min at room temperature, followed by the addition of primary MAb in the same blocking overnight at 4°C with constant gentle agitation. Following incubation with α-mouse IgG HRP-coupled secondary Abs (Jackson Immuno Research) at room temperature for 1 h, signals were visualized by chemiluminescence (ECL Prime Western Blotting Detection Reagent, Amersham, GE Healthcare or SuperSignal West Femto maximum sensitivity substrate; ThermoFisher) using ImageQuant LAS 4000 mini-instrument (GE Healthcare).

For Western blot analysis on virus preparations, the equal volume of virus stocks (normalized to contain equal amounts of infectious virus particle as determined by standard plaque assay described previously) were mixed directly with denaturing sample buffer, heated for 5 min at 95°C, and then loaded on 10% SDS-PAGE.

Affinity purified MAbs generated in-house (Center for Proteomics, University of Rijeka) used for Western blot are α–M116, α-m04 (m04.10, #HR-MCMV-01), α-gB (M55.01; #HR-MCMV-05), α-IE1 (IE1.01, #HR-MCMV-08), α-E1 (CROMA 103, #HR-MCMV-07), and α-CD63 (mCD63.07). For loading control, the MAb α-actin (clone C4; Merck) was used. MAbs generated by us in the Center for Proteomics are available from the Center for Proteomics website at https://products.capri.com.hr/.

Analysis of glycosylation. Endo H, PNGase F, and O-glycosidase treatments were performed according to the manufacturer's recommendations (New England Biolabs). Briefly, cell lysates in RIPA buffer were diluted with denaturing buffer and boiled for 10 min. Reaction buffer and enzyme were added, as well as NP40 (1%) to the PNGase F reaction or neuraminidase and NP40 (1%) to the O-glycosidase reaction, per manufacturers' instructions. The reaction mixture was incubated at 37°C for 1 h, and samples were then analyzed by Western blotting as described above.

Co-immunoprecipitation. WT^R-gH-HA-MCMV infected MEFs were lysed in lysis buffer (20 mM Tris-HCl pH 8.0, 150 mM NaCl, 1% Triton X-100) with the addition of protease inhibitor cocktail (cOmplete mini; Roche). Lysates were precleared with protein G Sepharose beads (GE Healthcare) and co-incubated with α-M116 or α-gH (8D122A; kindly provided by Lambert Loh, University of SK, Canada) MAbs under rotation at 4°C overnight. Then protein-MAb complexes were precipitated with protein G Sepharose beads under rotation for 4 h on +4°C and washed 3 times in lysis buffer. The precipitates were dissociated in sample buffer (0.13MTris-HCl (pH 6.8), 6% SDS, 10% a-thioglycerol), heated for 5 min at 95°C and

subjected to SDS-polyacrylamide gel electrophoresis (SDS-PAGE), followed by Western blotting analysis using nitrocellulose membranes (GE Healthcare) for protein transfer. The membranes were incubated with α-HA (3F10, Sigma-Aldrich, Germany) primary MAb and peroxidase-coupled α-rat secondary Ab (Jackson ImmunoResearch). The signals were visualized by Super Signal West Pico or SuperSignal West Femto chemiluminescence substrate (ThermoScientific) using Fusion FX instrument (Vilber).

Flow cytometry. For M116.1p surface expression analysis, primary MEFs infected with WT-MCMV and ΔM116-MCMV were stained at 30 hpi with α-M116 MAb followed by staining with α–mouse FITC MAb (Jackson ImmunoResearch). For intracellular M116.1p expression analysis, cells were fixed and permeabilized before staining with the same combination of primary and secondary Abs as described for surface staining. Irrelevant IgG1 isotype-matched control produced in-house was used as a negative control. Fixable Viability Dye (1,000×, Thermo Fisher Scientific) or propidium iodide (PI, Sigma-Aldrich) was used to stain dead cells. Intracellular staining, permeabilization, and fixation of cells were performed with the Fixation/Permeabilization kit (Thermo Fisher Scientific). All data were acquired using FACSAriaIIu (BD Biosciences) and analyzed using FlowJo software (TreeStar).

Proximity ligation assay (PLA). PLA was performed using Duolink flowPLA Green Detection Reagent (Sigma-Aldrich) according to the manufacturer's instructions. MEFs infected with WT^R-MCMV and WT^R-gH-HA-MCMV were collected 48 hpi, stained with Fixable Viability Dye (1,000×, Thermo Fisher Scientific), fixed with 4% PFA, permeabilized with ice-cold methanol, and labeled with MAbs α-M116 and α-HA (F-7, Santa Cruz). Because both MAbs used were from mice, α-M116 MAb was directly labeled with MINUS oligonucleotides using Duolink ProbeMaker kits (Sigma-Aldrich), according to the manufacturer's instructions. The cells were first stained with α-HA MAb, followed by α-mouse PLUS probe, and finally directly labeled α-M116-MINUS. Following oligonucleotide ligation, DNA amplification was left overnight and the detection was performed the following day. Cells were washed between each step. All data were acquired using FACSAria (BD Biosciences) and analyzed using FlowJo software (TreeStar).

Immunofluorescence microscopy. Primary BALB/c MEFs or Balb 3T3 fibroblasts were seeded on the glass coverslips in 12-well plates and the following day infected with 0.5 or 1 PFU/cell of WT-MCMV, ΔM116-MCMV, WT^R-gH-HA-MCMV, or Δm138-MCMV by incubating adherent cell layer for 30 min in 500 μl of virus suspension at 37°C and in an atmosphere with 5% CO_2, followed by 30 min centrifugation at 800 × *g* (centrifugal enhancement). In the indicated experiment, the cells were treated with BFA (3 μg/ml, eBioscience) for the last 12h of infection. Cells were fixed with 4% PFA, permeabilized with 0.1% Triton X-100 or 1% Tween20, and analyzed for target proteins localization at the indicated time p.i. The following in-house produced MAbs were used: α-M116 and α-IE1 (IE1.01, #HR-MCMV-08). The following purchased MAbs were used: α-HA (RM305, Thermo Fisher Scientific), α-HA (3F10, Roche), α-Rab6, α-Rab10 (Cell Signaling Tech., USA), and α-Rab31 (Sigma–Aldrich Chemie GmbH, Germany). For visualization of nuclei, PI and DAPI were used in some experiments. The samples were stained with appropriate isotype-specific secondary Abs coupled to fluorescein isothiocyanate (FITC), tetramethylrhodamine (TRITC), Alexa Fluor 488, Alexa Fluor 555, or Alexa Fluor 647 (Thermo Fischer Scientific, USA). To avoid the possibility of cross-reactivity, all secondary Ab reagents have been tested against primary MAbs and secondary Ab reagents that were used. Following staining, cells were mounted using mounting medium ProLong Gold Antifade Mountant or Mowiol (Fluka Chemicals, Selzee, Germany; Sigma Chemical Co, Steinheim, Germany) in PBS containing 50% glycerol and analyzed by Olympus Fluoview FV300 confocal microscope (Olympus Optical Co., Tokyo, Japan) and Ar 488, He/Ne 543, and He/Ne 633 lasers. Images were visualized and acquired by PLAPO60xO oil objective and Fluoview software, version 4.3 FV 300 (Olympus Optical Co., Tokyo, Japan). Appropriate barrier filters have been used during image acquisition, and confocal aperture was set to 2, PMT 600–800, beam splitter at 570 nm, without Kalman filtering. Fo co-localization following siRNA experiments, a DMi8 inverted microscope, and a confocal Leica Microsystem TCS SP8 were used, with LAS X software, and the use of a 405 diode laser and a RYB laser combination consisting of: blue Ar laser 458, yellow laser DPSS 561 nm, and red laser HeNe 633 nm.

The images were acquired in xyz sections (z series of 0.5 μm optical sections) in a sequential mode and with medium scan speed (1,65s/scan). The average number of slices was 8–14, and all-optical sections across the cell have been included. The offset has been set below 5% and adjusted to the signal in noninfected cells. In order to better visualize intracellular structures, we have used 2x, 4x, and ×8 magnifications.

The exported images (TIFF, 515 × 512 pixels) were analyzed with ImageJ software and available plugins (Plot Profile and JACoP). For colocalization analysis, 8× zoomed images have been used and analyzed with ImageJ 1.47v software, utilizing the JACoP plugin (http://rsb.info.nih.gov/ij/plugins/track/jacop.html) (Bolte and Cordeliéres, 2006). Manders' overlap coefficients (M1 and M2) have been calculated within the entire z-stack and after eliminating most of the signal background (Costes automatic thresholding method). Approximately 6–10 cells were analyzed. The plotting profiles for colocalization presentation have been achieved after analysis of focus sections. Finally, for 3D reconstruction, we have used ImageJ Volume Viewer plugin.

Immunohistochemistry analysis. Organs were harvested from BALB/c mice 4 days following i.v. infection with 2×10^5 PFU/mouse of WT-MCMV and ΔM116-MCMV and then fixated with 4% paraformaldehyde (PFA) for 2 days, embedded in paraffin, and then 2-μm thin liver sections were cut and processed for immunohistochemistry following standard protocol (114). After de-deparaffinization and rehydration, antigen retrieval was performed in sodium citrate buffer (pH 6.0) at 98°C for 20 min. Neighboring sections were stained for pp89/IE1 (IE1.01, #HR-MCMV-08) MCMV protein, as previously described (115) and with α-M116 MAb, followed by peroxidase-conjugated AffiniPure goat α-mouse IgG (Jackson ImmunoResearch) and streptavidin-POD (Roche). Substrate DAB chromogen (Dako) was used to visualize MAb binding, and counterstaining was performed with hematoxylin.

Animal experiments. All mice used in experiments were housed and bred under specific pathogen-free conditions at the Central Animal Facility of the Medical Faculty, University of Rijeka. Eight-to-twelve-wk-old mice were used in all experiments and were age- and sex-matched within experiments. All experiments were approved by the Animal Welfare Committee and Responsible Expert of the University of Rijeka, Faculty of Medicine, Rijeka, Croatia, as well as by the Veterinary Department of the Ministry of Agriculture, and have been performed under the Croatian Animal Protection Act, which has been matched with existing European Union legislation. Animals were randomly assigned to groups and housed in cages in groups, a maximum of six animals/cage. Animals belonging to the same experimental group were housed together and were not housed with animals from other experimental groups.

BALB/c mice were infected with 2×10^5 PFU/mouse of tissue culture-grown MCMV in a volume of 500 μl (i.v.) or 50 μl (f.p.) of pure DMEM or 20 μl of PBS (i.n.). Animals were sacrificed at indicated time points, organs were harvested, and the expression of viral proteins was determined by immunohistochemistry analysis, or viral titers were determined by plaque assay on MEFs in two technical replicates (18). Statistical significance was calculated by unpaired two-tailed Mann–Whitney U test using GraphPad Prism 9 software.

Data availability. Sequences of the primary transcripts M116 and M116-M114 have been deposited into NCBI GenBank with accession numbers OK149197 and OK149198, respectively.

ACKNOWLEDGMENTS

This publication was supported by the grant "Strengthening the Capacity of the Scientific Centre of Excellence CerVirVac for Research in Viral Immunology and Vaccinology," KK.01.1.1.01.0006, financed by the European Regional Development Fund (principal investigator S.J.; B.L., workpackage leader). The work of doctoral student T.R. has been fully supported by the "Young Researchers' Career Development Project—Training of Doctoral Students" of the Croatian Science Foundation, awarded to B.L. (grant no. DOK-2015-10). The funders had no role in study design, data collection, and interpretation, or the decision to submit the work for publication.

We thank K. Miklić, S. Malić, D. Rumora, E. Ražić, D. Rebić, M. Pajcur, L. Mikša, S. Stupac Slavić, N. Vragović, M. Trkulja, A. Miše, E. Marinović, and M. Samsa for the excellent technical support, K. Grabušić and O. Shevchuk for their work on α-CD63 MAbk, and Igor Jurak for the reagents. We thank Ilija Brizić and Melanie Brinkmann for the fruitful discussions. We also thank A. Gerbin, I. Nenadić, C. Paulović, A. Šarlija, and A. Novak for excellent administrative support.

REFERENCES

1. Forte E, Zhang Z, Thorp EB, Hummel M. 2020. Cytomegalovirus latency and reactivation: An intricate interplay with the host immune response. Front Cell Infect Microbiol 10:130. https://doi.org/10.3389/fcimb.2020.00130.
2. Boeckh M, Geballe AP. 2011. Cytomegalovirus: pathogen, paradigm, and puzzle. J Clin Invest 121:1673–1680. https://doi.org/10.1172/JCI45449.
3. Boppana SB, Ross SA, Fowler KB. 2013. Congenital cytomegalovirus infection: Clinical outcome. Clinical Infectious Diseases 57:S178–S181. https://doi.org/10.1093/cid/cit629.
4. Sinzger C, Digel M, Jahn G. 2008. Cytomegalovirus cell tropism. Curr Top Microbiol Immunol 325:63–83. https://doi.org/10.1007/978-3-540-77349-8_4.
5. Krmpotic A, Bubic I, Polic B, Lucin P, Jonjic S. 2003. Pathogenesis of murine cytomegalovirus infection. Microbes Infect 5:1263–1277. https://doi.org/10.1016/j.micinf.2003.09.007.
6. Gardner TJ, Tortorella D. 2016. Virion glycoprotein-mediated immune evasion by human cytomegalovirus: a sticky virus makes a slick getaway. Microbiol Mol Biol Rev 80:663–677. https://doi.org/10.1128/MMBR.00018-16.
7. Nguyen C, Kamil J. 2018. Pathogen at the gates: human cytomegalovirus entry and cell tropism. Viruses 10:704. https://doi.org/10.3390/v10120704.
8. Cui X, Snapper CM. 2019. Development of novel vaccines against human cytomegalovirus. Hum Vaccin Immunother 15:2673–2683. https://doi.org/10.1080/21645515.2019.1593729.
9. Anderholm KM, Bierle CJ, Schleiss MR. 2016. Cytomegalovirus vaccines: current status and future prospects. Drugs 76:1625–1645. https://doi.org/10.1007/s40265-016-0653-5.
10. Brinkmann MM, Dağ F, Hengel H, Messerle M, Kalinke U, Čičin-Šain L. 2015. Cytomegalovirus immune evasion of myeloid lineage cells. Med Microbiol Immunol 204:367–382. https://doi.org/10.1007/s00430-015-0403-4.
11. Lisnic B, Lisnic VJ, Jonjic S. 2015. NK cell interplay with cytomegaloviruses. Curr Opin Virol 15:9–18. https://doi.org/10.1016/j.coviro.2015.07.001.
12. Doom CM, Hill AB. 2008. MHC class I immune evasion in MCMV infection. Med Microbiol Immunol 197:191–204. https://doi.org/10.1007/s00430-008-0089-y.
13. Guilliams M, Ginhoux F, Jakubzick C, Naik SH, Onai N, Schraml BU, Segura E, Tussiwand R, Yona S. 2014. Dendritic cells, monocytes and macrophages: a unified nomenclature based on ontogeny. Nat Rev Immunol 14:571–578. https://doi.org/10.1038/nri3712.
14. Baasch S, Ruzsics Z, Henneke P. 2020. Cytomegaloviruses and macrophages—Friends and foes from early on? Front Immunol 11:793. https://doi.org/10.3389/fimmu.2020.00793.
15. Alexandre YO, Cocita CMD, Ghilas S, Dalod M. 2014. Deciphering the role of DC subsets in MCMV infection to better understand immune protection against viral infections. Front Microbiol 5:378. https://doi.org/10.3389/fmicb.2014.00378.
16. Sinclair J, Reeves M. 2014. The intimate relationship between human cytomegalovirus and the dendritic cell lineage. Front Microbiol 5:389.
17. Gordon S, Plüddemann A. 2019. The mononuclear phagocytic system: generation of diversity. Front Immunol 10:1893. https://doi.org/10.3389/fimmu.2019.01893.
18. Brizić I, Lisnić B, Brune W, Hengel H, Jonjić S. 2018. Cytomegalovirus infection: mouse model. Curr Protoc Immunol 122:e51. https://doi.org/10.1002/cpim.51.
19. Rawlinson WD, Farrell HE, Barrell BG. 1996. Analysis of the complete DNA sequence of murine cytomegalovirus. J Virol 70:8833–8849. https://doi.org/10.1128/JVI.70.12.8833-8849.1996.
20. Scalzo AA, Corbett AJ, Rawlinson WD, Scott GM, Degli-Esposti MA. 2007. The interplay between host and viral factors in shaping the outcome of cytomegalovirus infection. Immunol Cell Biol 85:46–54. https://doi.org/10.1038/sj.icb.7100013.

21. Wagner FM, Brizic I, Prager A, Trsan T, Arapovic M, Lemmermann NA, Podlech J, Reddehase MJ, Lemnitzer F, Bosse JB, Gimpfl M, Marcinowski L, MacDonald M, Adler H, Koszinowski UH, Adler B. 2013. The viral chemokine MCK-2 of murine cytomegalovirus promotes infection as part of a gH/gL/MCK-2 complex. PLoS Pathog 9:e1003493. https://doi.org/10.1371/journal.ppat.1003493.
22. Juranic Lisnic V, Babic Cac M, Lisnic B, Trsan T, Mefferd A, Das Mukhopadhyay C, Cook CH, Jonjic S, Trgovcich J. 2013. Dual Analysis of the Murine Cytomegalovirus and Host Cell Transcriptomes Reveal New Aspects of the Virus-Host Cell Interface. PLoS Pathog 9:e1003611. https://doi.org/10.1371/journal.ppat.1003611.
23. Marcinowski L, Lidschreiber M, Windhager L, Rieder M, Bosse JB, Rädle B, Bonfert T, György I, De Graaf M, Da Costa OP, Rosenstiel P, Friedel CC, Zimmer R, Ruzsics Z, Dölken L. 2012. Real-time transcriptional profiling of cellular and viral gene expression during lytic cytomegalovirus infection. PLoS Pathog 8:e1002908. https://doi.org/10.1371/journal.ppat.1002908.
24. Stern-Ginossar N, Weisburd B, Michalski A, Le VTK, Hein MY, Huang S-X, Ma M, Shen B, Qian S-B, Hengel H, Mann M, Ingolia NT, Weissman JS. 2012. Decoding human cytomegalovirus. Science 338:1088–1093. https://doi.org/10.1126/science.122791.9.
25. Nightingale K, Lin K-M, Ravenhill BJ, Davies C, Nobre L, Fielding CA, Ruckova E, Fletcher-Etherington A, Soday L, Nichols H, Sugrue D, Wang ECY, Moreno P, Umrania Y, Huttlin EL, Antrobus R, Davison AJ, Wilkinson GWG, Stanton RJ, Tomasec P, Weekes MP. 2018. High-definition analysis of host protein stability during human cytomegalovirus infection reveals antiviral factors and viral evasion mechanisms. Cell Host Microbe 24:447–460.e11. https://doi.org/10.1016/j.chom.2018.07.011.
26. Gatherer D, Seirafian S, Cunningham C, Holton M, Dargan DJ, Baluchova K, Hector RD, Galbraith J, Herzyk P, Wilkinson GWG, Davison AJ. 2011. High-resolution human cytomegalovirus transcriptome. Proc Natl Acad Sci U S A 108:19755–19760. https://doi.org/10.1073/pnas.1115861108.
27. Stingley SW, Ramirez JJG, Aguilar SA, Simmen K, Sandri-Goldin RM, Ghazal P, Wagner EK. 2000. Global analysis of herpes simplex virus type 1 transcription using an oligonucleotide-based DNA Microarray. J Virol 74:9916–9927. https://doi.org/10.1128/jvi.74.21.9916-9927.2000.
28. Harkness JM, Kader M, Deluca NA. 2014. Transcription of the herpes simplex virus 1 genome during productive and quiescent infection of neuronal and nonneuronal cells. J Virol 88:6847–6861. https://doi.org/10.1128/JVI.00516-14.
29. Caló S, Cortese M, Ciferri C, Bruno L, Gerrein R, Benucci B, Monda G, Gentile M, Kessler T, Uematsu Y, Maione D, Lilja AE, Carfí A, Merola M. 2016. The human cytomegalovirus UL116 gene encodes an envelope glycoprotein forming a complex with gH independently from gL. J Virol 90:4926–4938. https://doi.org/10.1128/JVI.02517-15.
30. Siddiquey MNA, Schultz EP, Yu Q, Amendola D, Vezzani G, Yu D, Maione D, Lanchy JM, Ryckman BJ, Merola M, Kamil JP. 2021. The human cytomegalovirus protein UL116 interacts with the viral ER resident glycoprotein UL148 and promotes the incorporation of gH/gL complexes into virions. J Virol 95. https://doi.org/10.1128/JVI.02207-20.
31. Gatault P, Jones IKA, Meyer C, Kreklywich C, Alexander T, Smith PP, Denton M, Powell J, Orloff SL, Streblow DN. 2021. Rat and human cytomegalovirus ORF116 encodes a virion envelope glycoprotein required for infectivity. Virology 557:23–33. https://doi.org/10.1016/j.virol.2020.12.014.
32. Vezzani G, Amendola D, Yu D, Chandramouli S, Frigimelica E, Maione D, Merola M. 2021. The human cytomegalovirus UL116 glycoprotein is a chaperone to control gH-based complexes levels on virions. Front Microbiol 12:630121. https://doi.org/10.3389/fmicb.2021.630121.
33. Redwood AJ, Masters LL, Chan B, Leary S, Forbes C, Jonjic S, Juranic Lisnic V, Lisnic B, Smith LM. 2020. Repair of an attenuated low-passage murine cytomegalovirus bacterial artificial chromosome identifies a novel spliced gene essential for salivary gland tropism. J Virol 94:e01456-20.
34. Chapa TJ, Perng YC, French AR, Yu D. 2014. Murine cytomegalovirus protein pM92 is a conserved regulator of viral late gene expression. J Virol 88:131–142. https://doi.org/10.1128/JVI.02684-13.
35. Chapa TJ, Johnson LS, Affolter C, Valentine MC, Fehr AR, Yokoyama WM, Yu D. 2013. Murine cytomegalovirus protein pM79 is a key regulator for viral late transcription. J Virol 87:9135–9147. https://doi.org/10.1128/JVI.00688-13.
36. Jiang LC, Schlesinger F, Davis CA, Zhang Y, Li RH, Salit M, Gingeras TR, Oliver B. 2011. Synthetic spike-in standards for RNA-seq experiments. Genome Res 21:1543–1551. https://doi.org/10.1101/gr.121095.111.
37. Mourão K, Schurch N, Lucoszek R, Froussios K, MacKinnon K, Duc C, Simpson G, Barton G. 2019. Detection and mitigation of spurious antisense expression with RoSA [version 1; peer review: 2 approved with reservations. F1000Res 8:819.]. https://doi.org/10.12688/f1000research.18952.1.
38. van Dijk EL, Jaszczyszyn Y, Thermes C. 2014. Library preparation methods for next-generation sequencing: tone down the bias. Exp Cell Res 322:12–20. https://doi.org/10.1016/j.yexcr.2014.01.008.
39. Zeng WH, Mortazavi A. 2012. Technical considerations for functional sequencing assays. Nat Immunol 13:802–807. https://doi.org/10.1038/ni.2407.
40. Wagner M, Jonjic S, Koszinowski UH, Messerle M. 1999. Systematic excision of vector sequences from the BAC-cloned herpesvirus genome during virus reconstitution. J Virol 73:7056–7060. https://doi.org/10.1128/JVI.73.8.7056-7060.1999.
41. Messerle M, Crnkovic I, Hammerschmidt W, Ziegler H, Koszinowski UH. 1997. Cloning and mutagenesis of a herpesvirus genome as an infectious bacterial artificial chromosome. Proc Natl Acad Sci U S A 94:14759–14763. https://doi.org/10.1073/pnas.94.26.14759.
42. Jordan S, Krause J, Prager A, Mitrovic M, Jonjic S, Koszinowski UH, Adler B. 2011. Virus progeny of murine cytomegalovirus bacterial artificial chromosome pSM3fr show reduced growth in salivary Glands due to a fixed mutation of MCK-2. J Virol 85:10346–10353. https://doi.org/10.1128/JVI.00545-11.
43. Garcia-Ortega L, Rios VD, Martinez-Ruiz A, Onaderra M, Lacadena J, del Pozo AM, Gavilanes JG. 2005. Anomalous electrophoretic behavior of a very acidic protein: Ribonuclease U2. Electrophoresis 26:3407–3413. https://doi.org/10.1002/elps.200500261.
44. Barnard DC, Patton JG. 2000. Identification and characterization of a novel serine-arginine-rich splicing regulatory protein. Mol Cell Biol 20:3049–3057. https://doi.org/10.1128/MCB.20.9.3049-3057.2000.
45. Tiwari P, Kaila P, Guptasarma P. 2019. Understanding anomalous mobility of proteins on SDS-PAGE with special reference to the highly acidic extracellular domains of human E- and N-cadherins. Electrophoresis 40:1273–1281. https://doi.org/10.1002/elps.201800219.
46. Graceffa P, Jancso A, Mabuchi K. 1992. Modification of acidic residues normalizes sodium dodecyl-sulfate polyacrylamide-gel electrophoresis of caldesmon and other proteins that migrate anomalously. Arch Biochem Biophys 297:46–51. https://doi.org/10.1016/0003-9861(92)90639-e.
47. Alves VS, Pimenta DC, Sattlegger E, Castilho BA. 2004. Biophysical characterization of Gir2, a highly acidic protein of Saccharomyces cerevisiae with anomalous electrophoretic behavior. Biochem Biophys Res Commun 314:229–234. https://doi.org/10.1016/j.bbrc.2003.12.086.
48. Taherzadeh G, Dehzangi A, Golchin M, Zhou Y, Campbell MP. 2019. SPRINT-Gly: predicting N- and O-linked glycosylation sites of human and mouse proteins by using sequence and predicted structural properties. Bioinformatics 35:4140–4146. https://doi.org/10.1093/bioinformatics/btz215.
49. Kleijnen MF, Huppa JB, Lucin P, Mukherjee S, Farrell H, Campbell AE, Koszinowski UH, Hill AB, Ploegh HL. 1997. A mouse cytomegalovirus glycoprotein, gp34, forms a complex with folded class I MHC molecules in the ER which is not retained but is transported to the cell surface. EMBO J 16:685–694. https://doi.org/10.1093/emboj/16.4.685.
50. Smith LM, Shellam GR, Redwood AJ. 2006. Genes of murine cytomegalovirus exist as a number of distinct genotypes. Virology 352:450–465. https://doi.org/10.1016/j.virol.2006.04.031.
51. Boratyn GM, Camacho C, Cooper PS, Coulouris G, Fong A, Ma N, Madden TL, Matten WT, McGinnis SD, Merezhuk Y, Raytselis Y, Sayers EW, Tao T, Ye J, Zaretskaya I. 2013. BLAST: a more efficient report with usability improvements. Nucleic Acids Res 41:W29–33. https://doi.org/10.1093/nar/gkt282.
52. Edgar RC. 2004. MUSCLE: a multiple sequence alignment method with reduced time and space complexity. BMC Bioinformatics 5:113. https://doi.org/10.1186/1471-2105-5-113.
53. Čížková D, Baird SJE, Těšíková J, Voigt S, Ľudovít Ď, Piálek J, Goüy de Bellocq J. 2018. Host subspecific viral strains in European house mice: Murine cytomegalovirus in the Eastern (*Mus musculus musculus*) and Western house mouse (*Mus musculus domesticus*). Virology 521:92–98. https://doi.org/10.1016/j.virol.2018.05.023.
54. Kutle I, Sengstake S, Templin C, Glaß M, Kubsch T, Keyser KA, Binz A, Bauerfeind R, Sodeik B, Čičin-Šain L, Dezeljin M, Messerle M. 2017. The M25 gene products are critical for the cytopathic effect of mouse cytomegalovirus. Sci Rep 7:15588. https://doi.org/10.1038/s41598-017-15783-x.
55. Lučin P, Jug Vučko N, Karleuša L, Mahmutefendić Lučin H, Blagojević Zagorac G, Lisnić B, Pavišić V, Marcelić M, Grabušić K, Brizić I, Lukanović Jurić S. 2020. Cytomegalovirus generates assembly compartment in the early phase of infection by perturbation of host-cell factors recruitment at the early endosome/endosomal recycling compartment/trans-golgi interface. Front Cell Dev Biol 8:914.

56. Rodriguez-Gabin AG, Yin X, Si Q, Larocca JN. 2009. Transport of mannose-6-phosphate receptors from the trans-Golgi network to endosomes requires Rab31. Exp Cell Res 315:2215–2230. https://doi.org/10.1016/j.yexcr.2009.03.020.
57. Kattenhorn LM, Mills R, Wagner M, Lomsadze A, Makeev V, Borodovsky M, Ploegh HL, Kessler BM. 2004. Identification of proteins associated with murine cytomegalovirus virions. J Virol 78:11187–11197. https://doi.org/10.1128/JVI.78.20.11187-11197.2004.
58. Zhou Y, Mcnamara RP, Dittmer DP. 2020. Purification methods and the presence of RNA in virus particles and extracellular vesicles. Viruses 12:917. https://doi.org/10.3390/v12090917.
59. Nolte-'T Hoen E, Cremer T, Gallo RC, Margolis LB. 2016. Extracellular vesicles and viruses: Are they close relatives? Proc Natl Acad Sci U S A 113:9155–9161. https://doi.org/10.1073/pnas.1605146113.
60. Almagro Armenteros JJ, Tsirigos KD, Sønderby CK, Petersen TN, Winther O, Brunak S, Von Heijne G, Nielsen H. 2019. SignalP 5.0 improves signal peptide predictions using deep neural networks. Nat Biotechnol 37:420–423. https://doi.org/10.1038/s41587-019-0036-z.
61. Chardin P, McCormick F. 1999. Brefeldin A: the advantage of being uncompetitive. Cell 97:153–155. https://doi.org/10.1016/s0092-8674(00)80724-2.
62. Escola J-M, Kleijmeer MJ, Stoorvogel W, Griffith JM, Yoshie O, Geuze HJ. 1998. Selective enrichment of tetraspan proteins on the internal vesicles of multivesicular endosomes and on exosomes secreted by human B-lymphocytes. J Biol Chem 273:20121–20127. https://doi.org/10.1074/jbc.273.32.20121.
63. Turner DL, Korneev DV, Purdy JG, De Marco A, Mathias RA. 2020. The host exosome pathway underpins biogenesis of the human cytomegalovirus virion. Elife 9[CrossRef]. https://doi.org/10.7554/eLife.58288.
64. Bagchi S, Fredriksson R, Wallén-Mackenzie Å. 2015. In situ proximity ligation assay (PLA). Methods Mol Biol 1318:149–159. https://doi.org/10.1007/978-1-4939-2742-5_15.
65. Fredriksson S, Gullberg M, Jarvius J, Olsson C, Pietras K, Gustafsdottir SM, Ostman A, Landegren U. 2002. Protein detection using proximity-dependent DNA ligation assays. Nat Biotechnol 20:473–477. https://doi.org/10.1038/nbt0502-473.
66. Scrivano L, Esterlechner J, Mühlbach H, Ettischer N, Hagen C, Grünewald K, Mohr CA, Ruzsics Z, Koszinowski U, Adler B. 2010. The m74 gene product of murine cytomegalovirus (MCMV) is a functional homolog of human CMV gO and determines the entry pathway of MCMV. J Virol 84:4469–4480. https://doi.org/10.1128/JVI.02441-09.
67. Scrivano L, Sinzger C, Nitschko H, Koszinowski UH, Adler B. 2011. HCMV spread and cell tropism are determined by distinct virus populations. PLoS Pathog 7:e1001256. https://doi.org/10.1371/journal.ppat.1001256.
68. Li G, Nguyen CC, Ryckman BJ, Britt WJ, Kamil JP. 2015. A viral regulator of glycoprotein complexes contributes to human cytomegalovirus cell tropism. Proc Natl Acad Sci U S A 112:4471–4476. https://doi.org/10.1073/pnas.1419875112.
69. Ebermann L, Ruzsics Z, Guzmán CA, Van Rooijen N, Casalegno-Garduño R, Koszinowski U, Čičin-Šain L. 2012. Block of death-receptor apoptosis protects mouse cytomegalovirus from macrophages and is a determinant of virulence in immunodeficient hosts. PLoS Pathog 8:e1003062. https://doi.org/10.1371/journal.ppat.1003062.
70. Singhal PK, Sassi S, Lan L, Au P, Halvorsen SC, Fukumura D, Jain RK, Seed B. 2016. Mouse embryonic fibroblasts exhibit extensive developmental and phenotypic diversity. Proc Natl Acad Sci U S A 113:122–127. https://doi.org/10.1073/pnas.1522401112.
71. Helft J, Böttcher J, Chakravarty P, Zelenay S, Huotari J, Schraml BU, Goubau D, Sousa E, Reis C. 2015. GM-CSF mouse bone marrow cultures comprise a heterogeneous population of CD11c+MHCII+ macrophages and dendritic cells. Immunity 42:1197–1211. https://doi.org/10.1016/j.immuni.2015.05.018.
72. Na YR, Jung D, Gu GJ, Seok SH. 2016. GM-CSF grown bone marrow derived cells are composed of phenotypically different dendritic cells and macrophages. Mol Cells 39(10):734–741. https://doi.org/10.14348/molcells.2016.0160.
73. Stoddart CA, Cardin RD, Boname JM, Manning WC, Abenes GB, Mocarski ES. 1994. Peripheral blood mononuclear phagocytes mediate dissemination of murine cytomegalovirus. J Virol 68:6243–6253. https://doi.org/10.1128/JVI.68.10.6243-6253.1994.
74. Hsu KM, Pratt JR, Akers WJ, Achilefu SI, Yokoyama WM. 2009. Murine cytomegalovirus displays selective infection of cells within hours after systemic administration. J Gen Virol 90:33–43. https://doi.org/10.1099/vir.0.006668-0.
75. Collins TM, Quirk MR, Jordan MC. 1994. Biphasic viremia and viral gene expression in leukocytes during acute cytomegalovirus infection of mice. J Virol 68:6305–6311. https://doi.org/10.1128/JVI.68.10.6305-6311.1994.
76. Farrell HE, Davis-Poynter N, Bruce K, Lawler C, Dolken L, Mach M, Stevenson PG. 2015. Lymph node macrophages restrict murine cytomegalovirus dissemination. J Virol 89:7147–7158. https://doi.org/10.1128/JVI.00480-15.
77. Farrell HE, Bruce K, Lawler C, Oliveira M, Cardin R, Davis-Poynter N, Stevenson PG. 2017. Murine cytomegalovirus spreads by dendritic cell recirculation. mBio 8.[CrossRef]. https://doi.org/10.1128/mBio.01264-17.
78. Farrell HE, Bruce K, Lawler C, Stevenson PG. 2019. Murine cytomegalovirus spread depends on the infected myeloid cell type. J Virol 93:e00540-19.
79. Marquardt A, Halle S, Seckert CK, Lemmermann NAW, Veres TZ, Braun A, Maus UA, Förster R, Reddehase MJ, Messerle M, Busche A. 2011. Single cell detection of latent cytomegalovirus reactivation in host tissue. J Gen Virol 92:1279–1291. https://doi.org/10.1099/vir.0.029827-0.
80. Koffron AJ, Hummel M, Patterson BK, Yan S, Kaufman DB, Fryer JP, Stuart FP, Abecassis MI. 1998. Cellular localization of latent murine cytomegalovirus. J Virol 72:95–103. https://doi.org/10.1128/JVI.72.1.95-103.1998.
81. Reddehase M, Lemmermann N. 2018. Mouse model of cytomegalovirus disease and immunotherapy in the immunocompromised host: predictions for medical translation that survived the "test of time." Viruses 10:693. https://doi.org/10.3390/v10120693.
82. Ding F, Elowitz MB. 2019. Constitutive splicing and economies of scale in gene expression. Nat Struct Mol Biol 26:424–432. https://doi.org/10.1038/s41594-019-0226-x.
83. Thiel N, Keyser KA, Lemmermann NA, Oduro JD, Wagner K, Elsner C, Halenius A, Lenac Rovis T, Brinkmann MM, Jonjic S, Cicin-Sain L, Messerle M. 2016. The mouse cytomegalovirus gene m42 targets surface expression of the protein tyrosine phosphatase CD45 in infected macrophages. PLoS Pathog 12:e1006057. https://doi.org/10.1371/journal.ppat.1006057.
84. Ryckman BJ, Chase MC, Johnson DC. 2010. Human cytomegalovirus TR strain glycoprotein O acts as a chaperone promoting gH/gL incorporation into virions but is not present in virions. J Virol 84:2597–2609. https://doi.org/10.1128/JVI.02256-09.
85. Farrell H, Oliveira M, Macdonald K, Yunis J, Mach M, Bruce K, Stevenson P, Cardin R, Davis-Poynter N. 2016. Luciferase-tagged wild-type and tropism-deficient mouse cytomegaloviruses reveal early dynamics of host colonization following peripheral challenge. J Gen Virol 97:3379–3391. https://doi.org/10.1099/jgv.0.000642.
86. Hanson LK, Slater JS, Cavanaugh VJ, Newcomb WW, Bolin LL, Nelson CN, Fetters LD, Tang Q, Brown JC, Maul GG, Campbell AE. 2009. Murine cytomegalovirus capsid assembly is dependent on US22 family gene M140 in infected macrophages. J Virol 83:7449–7456. https://doi.org/10.1128/JVI.00325-09.
87. Hanson LK, Slater JS, Karabekian Z, Ciocco-Schmitt G, Campbell AE. 2001. Products of US22 genes M140 and M141 confer efficient replication of murine cytomegalovirus in macrophages and spleen. J Virol 75:6292–6302. https://doi.org/10.1128/JVI.75.14.6292-6302.2001.
88. Farrell HE, Lawler C, Tan CSE, Macdonald K, Bruce K, Mach M, Davis-Poynter N, Stevenson PG. 2016. Murine cytomegalovirus exploits olfaction to enter new hosts. mBio 7:e00251-16–e00216. https://doi.org/10.1128/mBio.00251-16.
89. Stahl FR, Heller K, Halle S, Keyser KA, Busche A, Marquardt A, Wagner K, Boelter J, Bischoff Y, Kremmer E, Arens R, Messerle M, Forster R. 2013. Nodular inflammatory foci are sites of T cell priming and control of murine cytomegalovirus infection in the neonatal lung. PLoS Pathog 9:e1003828. https://doi.org/10.1371/journal.ppat.1003828.
90. Stahl FR, Keyser KA, Heller K, Bischoff Y, Halle S, Wagner K, Messerle M, Forster R. 2015. Mck2-dependent infection of alveolar macrophages promotes replication of MCMV in nodular inflammatory foci of the neonatal lung. Mucosal Immunol 8:57–67. https://doi.org/10.1038/mi.2014.42.
91. Jordan MC. 1978. Interstitial pneumonia and subclinical infection after intranasal inoculation of murine cytomegalovirus. Infect Immun 21:275–280. https://doi.org/10.1128/iai.21.1.275-280.1978.
92. Farrell HE, Lawler C, Oliveira MT, Davis-Poynter N, Stevenson PG. 2016. Alveolar macrophages are a prominent but nonessential target for murine cytomegalovirus infecting the lungs. J Virol 90:2756–2766. https://doi.org/10.1128/JVI.02856-15.
93. Yunis J, Farrell HE, Bruce K, Lawler C, Sidenius S, Wyer O, Davis-Poynter N, Stevenson PG. 2018. Murine cytomegalovirus degrades MHC class II to colonize the salivary glands. PLoS Pathog 14:e1006905. https://doi.org/10.1371/journal.ppat.1006905.

94. Daley-Bauer LP, Roback LJ, Wynn GM, Mocarski ES. 2014. Cytomegalovirus hijacks CX3CR1(hi) patrolling monocytes as immune-privileged vehicles for dissemination in mice. Cell Host Microbe 15:351–362. https://doi.org/10.1016/j.chom.2014.02.002.
95. Zimmermann A, Trilling M, Wagner M, Wilborn M, Bubic I, Jonjic S, Koszinowski U, Hengel H. 2005. A cytomegaloviral protein reveals a dual role for STAT2 in IFN-{gamma} signaling and antiviral responses. J Exp Med 201:1543–1553. https://doi.org/10.1084/jem.20041401.
96. Ménard C, Wagner M, Ruzsics Z, Holak K, Brune W, Campbell AE, Koszinowski UH. 2003. Role of murine cytomegalovirus US22 gene family members in replication in macrophages. J Virol 77:5557–5570. https://doi.org/10.1128/jvi.77.10.5557-5570.2003.
97. Mack C, Sickmann A, Lembo D, Brune W. 2008. Inhibition of proinflammatory and innate immune signaling pathways by a cytomegalovirus RIP1-interacting protein. Proc Natl Acad Sci U S A 105:3094–3099. https://doi.org/10.1073/pnas.0800168105.
98. Daley-Bauer LP, Roback L, Crosby LN, McCormick AL, Feng Y, Kaiser WJ, Mocarski ES. 2017. Mouse cytomegalovirus M36 and M45 death suppressors cooperate to prevent inflammation resulting from antiviral programmed cell death pathways. Proc Natl Acad Sci U S A 114:E2786–E2795. https://doi.org/10.1073/pnas.1616829114.
99. Oliveira SA, Shenk TE. 2001. Murine cytomegalovirus M78 protein, a G protein-coupled receptor homologue, is a constituent of the virion and facilitates accumulation of immediate-early viral mRNA. Proc Natl Acad Sci U S A 98:3237–3242. https://doi.org/10.1073/pnas.051629898.
100. Puhach O, Ostermann E, Krisp C, Frascaroli G, Schlüter H, Brinkmann MM, Brune W. 2020. Murine cytomegaloviruses m139 targets DDX3 to curtail interferon production and promote viral replication. PLoS Pathog 16:e1008546. https://doi.org/10.1371/journal.ppat.1008546.
101. Chan B, Goncalves Magalhaes V, Lemmermann NAW, Juranic Lisnic V, Stempel M, Bussey KA, Reimer E, Podlech J, Lienenklaus S, Reddehase MJ, Jonjic S, Brinkmann MM. 2017. The murine cytomegalovirus M35 protein antagonizes type I IFN induction downstream of pattern recognition receptors by targeting NF-kappaB mediated transcription. PLoS Pathog 13:e1006382. https://doi.org/10.1371/journal.ppat.1006382.
102. Crnkovic-Mertens I, Messerle M, Milotic I, Szepan U, Kucic N, Krmpotic A, Jonjic S, Koszinowski UH. 1998. Virus attenuation after deletion of the cytomegalovirus Fc receptor gene is not due to antibody control. J Virol 72:1377–1382. https://doi.org/10.1128/JVI.72.2.1377-1382.1998.
103. Booth TW, Scalzo AA, Carrello C, Lyons PA, Farrell HE, Singleton GR, Shellam GR. 1993. Molecular and biological characterization of new strains of murine cytomegalovirus isolated from wild mice. Arch Virol 132:209–220. https://doi.org/10.1007/BF01309855.
104. Smith LM, Mcwhorter AR, Masters LL, Shellam GR, Redwood AJ. 2008. Laboratory Strains of murine cytomegalovirus are genetically similar to but phenotypically distinct from wild strains of virus. J Virol 82:6689–6696. https://doi.org/10.1128/JVI.00160-08.
105. Smith LM, McWhorter AR, Shellam GR, Redwood AJ. 2013. The genome of murine cytomegalovirus is shaped by purifying selection and extensive recombination. Virology 435:258–268. https://doi.org/10.1016/j.virol.2012.08.041.
106. Tischer BK, Smith GA, Osterrieder N. 2010. En passant mutagenesis: a two step markerless red recombination system. Methods Mol Biol 634:421–430. https://doi.org/10.1007/978-1-60761-652-8_30.
107. Železnjak J, Lisnić VJ, Popović B, Lisnić B, Babić M, Halenius A, L'Hernault A, Roviš TL, Hengel H, Erhard F, Redwood AJ, Vidal SM, Dölken L, Krmpotić A, Jonjić S. 2019. The complex of MCMV proteins and MHC class I evades NK cell control and drives the evolution of virus-specific activating Ly49 receptors. J Exp Med 216:1809–1827. https://doi.org/10.1084/jem.2018221.3.
108. Aranda PS, LaJoie DM, Jorcyk CL. 2012. Bleach gel: a simple agarose gel for analyzing RNA quality. Electrophoresis 33:366–369. https://doi.org/10.1002/elps.201100335.
109. Dobin A, Davis CA, Schlesinger F, Drenkow J, Zaleski C, Jha S, Batut P, Chaisson M, Gingeras TR. 2013. STAR: ultrafast universal RNA-seq aligner. Bioinformatics 29:15–21. https://doi.org/10.1093/bioinformatics/bts635.
110. Dobin A, Gingeras TR. 2016. Optimizing RNA-Seq Mapping with STAR, p 245–262. *In* Carugo O., Eisenhaber F. (ed), Data mining techniques for the life sciences: methods in molecular biology, vol 1415. Humana Press, New York, NY. https://doi.org/10.1007/978-1-4939-3572-7_13.
111. Li H, Handsaker B, Wysoker A, Fennell T, Ruan J, Homer N, Marth G, Abecasis G, Durbin R, 1000 Genome Project Data Processing Subgroup. 2009. The Sequence Alignment/Map format and SAMtools. Bioinformatics 25:2078–2079. https://doi.org/10.1093/bioinformatics/btp352.
112. Thorvaldsdottir H, Robinson JT, Mesirov JP. 2013. Integrative Genomics Viewer (IGV): high-performance genomics data visualization and exploration. Brief Bioinform 14:178–192. https://doi.org/10.1093/bib/bbs017.
113. Yokoyama WM, Christensen M, Dos Santos G, Miller D, Ho J, Wu T, Dziegelewski M, Neethling FA. 2013. Production of monoclonal antibodies. Curr Protoc Immunol 102:Unit 2.5.
114. Cekinovic D, Lisnic VJ, Jonjic S. 2014. Rodent models of congenital cytomegalovirus infection. Methods Mol Biol 1119:289–310. https://doi.org/10.1007/978-1-62703-788-4_16.
115. Keil GM, Ebeling-Keil A, Koszinowski UH. 1987. Immediate-early genes of murine: location, transcripts, and translation products. J Virol 61:526–533. https://doi.org/10.1128/JVI.61.2.526-533.1987.